QATAR UNIVERSITY

COLLEGE OF ENGINEERING

DEVELOPMENT OF AIR-JET SPUN PHBV/PCL COMPOSITE SCAFFOLDS FOR WOUND HEALING APPLICATIONS

BY

NUTHANA KALVA SUMAMA

A Thesis Submitted to

the College of Engineering

in Partial Fulfillment of the Requirements for the Degree of

Master of Science in Mechanical Engineering

June 2021

COMMITTEE PAGE

The members of the Committee approve the Thesis of
Nuthana kalva Sumama defended on 10/05/2021.

MD Anwarul Hasan
Thesis/Dissertation Supervisor

Wojciech Swieszkowsk
Committee Member

Faris Tarlochan
Committee Member

Khaled MD Khan
Committee Member

Approved:

Khalid Kamal Naji, Dean, College of Engineering

ABSTRACT

NUTHANA KALVA SUMAMA, Masters:

June : 2021, Masters of Science in Mechanical Engineering

Title: Development of air-jet spun PHBV/PCL composite scaffolds for wound healing applications

Supervisor of Thesis: Dr Anwarul Hasan.

Delay in the healing of chronic wounds is one of the major problems causing individuals to lose their lives and which also becomes a severe burden on the nation's healthcare. Nanotechnology has allowed the development of low-priced wound-covering materials, like nanofibrous materials, that have high surface-to-to-volume ratios to be made in wide varieties of shapes and sizes.

The first aim of this research is to find the best PHBV/PCL blend ratio for fabricating fibrous mats through air-jet spinning for wound healing applications. Different ratios of PHBV and PCL (100 % PCL, 30/70, 50/50, 70/30, 100 % PHBV) were investigated for this reason. SEM data shows that the fiber diameters varied in the sub-nanometer scale. The crystallinity of the fibers increased as the PCL content increased, according to the XRD data. In comparison to pure PHBV and PCL, PHBV/PCL 50/50 demonstrated better combination of cell proliferation and mechanical strength than pure PHBV.

The second aim is to study the effect of incorporating curcumin as an active agent into the optimized blend on wound healing. The optimized PHBV/PCL composition was mixed with different curcumin concentrations (0.5, 1, 2, 3 & 5 %). On the loaded fibers, physio-mechanical characterizations were performed to assess the impact of nanoparticle incorporation. Also, the cytotoxicity and cell migration

studies were carried out to find out the cell proliferation activity. Our findings indicate that 0.5 % curcumin-loaded PHBV/PCL fibers have promising wound healing potential.

DEDICATION

I would like to dedicate this thesis to

my parents without whom I would not be where I am today.

Finally, I would like to express my gratitude to Dr. Anwarul Hasan and

Dr. Robin Augustine who have been extremely supportive

from the beginning of my research and for their help and guidance in

completing this thesis.

ACKNOWLEDGMENTS

This project was completed at Qatar University's Mechanical and Industrial Engineering Department. The author wishes to express his gratitude to the university and the department for their support of the project.

I thank the Qatar University's Biomedical Research Center (BRC), Center of Advanced Materials (CAM), and Central Lab Unit (CLU) for enabling us to conduct research in their labs.

The author would like to acknowledge the financial support of the Qatar National Research Fund (a member of Qatar Foundation) through the National Priorities Research Program NPRP 10 – 0120 – 170211.

ABBREVIATIONS

PHBV	Poly(3-hydroxybutyrate-co-3-hydroxyvalerate)
PCL	Polycaprolactone
Cur	Curcumin
SEM	Scanning electron microscope
FTIR	Fourier-transform infrared spectroscopy
XRD	X-ray diffraction
DSC	Differential Scanning Calorimetry
TGA	Thermogravimetric analysis
UV	Ultraviolet
DPBS	Dulbecco’s Phosphate buffered saline
DMEM	Dulbecco's Modified Eagle Medium

TABLE OF CONTENTS

LIST OF TABLES

LIST OF FIGURES

CHAPTER 1: Introduction

1.1 Background

Currently, delays in the cure of chronic injuries are a key concern, resulting in higher budgets on one side and an impaired quality of life on the other. 60–80% of all human infectious illnesses include chronic infections, including chronic wounds [1], [2]. Diabetic ulcers are a major cause of chronic wounds. Wound healing is often hampered by several factors including microbial infections, deceased growth factors secretion, and poor supply of oxygen and nutrients to the cells replacing damaged tissue. Healing of wound include migration and proliferation of the cells as well as secretion of growth factors and hormones which are accomplished during hemostasis, inflammation, proliferation and maturation phases of damaged tissue recovery[3], [4]. The time of recovery depends upon the complexity of the wound such as acute or chronic wound.

Acute wounds are treated with standard treatment procedures, such as swabbing to remove infections, cleaning, dressing, and in some cases debridement of the wound. However, using these treatment options especially during old age cause accumulation of bacteria film1 which results in delay in healing of wounds. In this way, an acute wound may turn into a chronic wound. Moreover, the size of wound damage is an important factor in regeneration and the development of new tissues. A wound in epidermis (upper skin layer) or dermis (middle layer of skin) less than 1 cm area can heal faster as the skin possess enough potential to replace this damaged tissue. However, a deep injury in dermis and hypodermis area of skin results in delayed recovery of skin and require a patch of skin to be substituted in order to speed up the regeneration process[5], [6].

Therefore, scientists have focused their attention in the development of new and novel types of wound healing patches for the quicker and faster healing of wound[7]. In

this direction, biodegradables polymers could be favorable materials to be used as tissue engineered scaffolds, heart values and cardiovascular tissues, and orthopedic and intestinal anastomosis devices. However, selection of these materials is very important as sometime these biomaterials may lead to cell deaths and revoke the cell regeneration process. In addition, these agents may provoke foreign body response and may lead to platelet activation. These immunogenic reactions mostly restrict the use of these materials as they initiate various bio responses that posed various complications and may be hazardous to the patient life. Therefore, using advanced bio interactive and biocompatible materials that will help in the cell proliferation, migration and healing of the wound are recommended for biomedical applications especially for wound healing[8]–[11].

Various synthetic and natural skin patches are available in the market that has been used in the healing of wounds. However, their use has been hampered by several factors including high cost, minimal effect on healing time and limited recovery of wound area due to their functionalities. Biomaterials that possess high swelling capability for absorbing extra exudates, highly porous structure and are permeable to oxygen can be one of amazing candidates for faster recovery and regeneration of damaged tissues. These traits may enable the faster healing and steadily delivery of insulin to remove bacteria and infections without posing any side effects. Membranes have already shown its promising application in wound healing that provides suitable environment. In terms of physical characteristics, it provides continuous and flexible micro and nano structure, good swelling capability, and can easy be mold in different shapes. While in terms of biological responses, it is highly biocompatible with the human tissue, biodegradable, nontoxic, provides controlled release of drugs and proteins and highly favorable in tissue engineering applications[12]–[14].

1.2 Aims and objectives of the study

The first aim of this study is to develop stronger and biologically more viable fiber mats through air-jet spinning. To achieve this, we propose to fabricate composite fiber mats of PHBV and PCL. Different blends of PHBV/PCL fiber mats were fabricated and characterized to assess the effects of blending on the physio-mechanical as well as biological properties of the samples. The blend showing the best combination of biological and mechanical properties was selected for further studies.

The second aim is to study the effect of incorporating curcumin as an active agent into the best blend from the first study. The PHBV/PCL blend was mixed with different curcumin concentrations. On the loaded fibers, physio-mechanical and cell culture studies were performed to assess the influence of nanoparticle incorporation.

1.3 Overview of thesis

This thesis is divided into five chapters. The sequence of the chapters are as below:

Chapter 1 introduces the background and significance of the problem. The aims and objectives of the study are discussed in detail. The chapter then lays out the overview of the thesis.

Chapter 2 presents the detailed literature review of various fabrication techniques being used for fabrication of biomaterials for wound healing applications. It opens the avenue of recent use of air-jet spinning for fibrous biomaterials for wound healing applications. Following this, PCL, PHBV and the blend of PCL\PHBV membranes for wound healing applications were explored. Furthermore, the role of Curcumin was thoroughly described in terms of wound healing. Moreover, it includes benefits and behavior of Curcumin on wound healing.

Chapter 3 explains the materials and methods to fabricate the PCL\PHBV

membranes incorporated Curcumin membranes. After then, it describes the physical characterization approaches, then the biological characterizations using the cell culture investigation in an *In vitro model.*

Chapter 4 is divided into two parts. The first part presents the thorough analysis of different compositions of PCL\PHBV to find the best ratio of composition of PCL and PHBV to achieve optimum mechanical and biological properties. The second part presents the detailed and thoroughly analysis of incorporating different concentrations of Curcumin in the optimized composition of PCL\PHBV from the above study.

Chapter 5 concludes the present study with the promising potential of Curcumin loaded PCL\PHBV as a wound healing membrane. In addition, it further defines the future work recommendations in order to investigate its viability in *in vivo* models.

CHAPTER 2: LITERATURE REVIEW

2.1 Methods for the development of wound healing materials

The selection of fabrication technique along with the choice of material determine the properties of the resulting scaffolds. Although many approaches have been investigated to increase porosity of the scaffolds and limit the ingrowth of cells, these methods have not been able to produce scaffolds of reasonable thickness to be considered as 3D scaffolds [15]. The following section briefly describes the various conventional as well as modern techniques that are being used for the development of scaffolds for wound healing applications.

*Self-assembly***:** The property of autonomous organization of components into structures and patterns, known as self-assembly, can be utilized for fabrication of ECM mimetic structures. Various complex, highly specific non-covalent interactions drive the assembly of structures like micelle/bilayer lipids, and α-helix and β-sheet structural motifs of proteins [16], [17]. This method produces fibers having diameters in the range of tens of nanometers. The assembling mechanisms are initiated through mixing of components or by an external stimulus like change in pH, temperature, etc. [18], [19]. This makes it possible to directly encapsulate cells, which is easier in comparison to other fabrication methods that require sophisticated instruments. But the mechanisms governing the self-assembly are more complicated and therefore require careful and complex experimental design. Scaffolds produced by self-assembly of proteins and peptides which have been shown to mimic the natural ECM. Various studies have demonstrated the enhanced cell adhesion, proliferation and differentiation of mammalian cells on self-assembled-oligopeptide based scaffolds [20]–[22]. Despite the many advantages, matrices fabricated by this approach show poor mechanical strength and the fragmented fibers pose the threat of endocytosis. Along with these drawbacks, the high

cost of synthesis restricts their applications in tissue engineering and regenerative medicine [23].

*Thermally induced phase separation***:** The thermal energy difference during a quenching process is utilized to initiate the void formation in a homogenous polymer solution. After exposing the solubilized polymer to high temperatures, the temperature is rapidly decreased to prompt the phase separation. By strong fluid de-blending, the solution then forms polymer-free phase and solvent-free phase. In this technique, the scaffolds microstructure can be manipulated by controlling the polymer properties, solvents and the working temperature [24]. The phase separation can be carried out either between solid-liquid or liquid-liquid phase. This technique offers the benefit of compatibility with many of the other manufacturing techniques and gives superior mechanical properties with controlled porous structure.

*Melt molding***:** Melt-based fabrication methods are derived from the conventional polymer fabrication methods. However, these methods are then coupled with pore-generating techniques to generate porosity in the material [25]. Generally, water soluble salts are mixed with polymer during molding and the salts are dissolved in water after molding leading to a porous structure. The advantages of this process is that toxic solvents are avoided and the pore size can also be controlled by using porogens of suitable size [25]. By combining with techniques like particle leaching, gas foaming and use of porogens, this method shows great potential for the generation of ECM-mimetic tissue regeneration studies.

*Gas foaming***:** This technique uses a foaming agent with the polymer. To initiate the nucleation and develop the gas rise in the substance, high pressure gas is applied on the disks of polymer. These are then lyophilized to generate scaffolds having pore sizes in the range of 100 μm and porosity of about 93% after releasing of gases [26]. The

formation of gas is due to reaction of foaming agent with the acidic solution producing porous structure. This procedure has great reliability to create solvents-free scaffolds. But the heterogeneity of the structure having irregular porosity is the major disadvantage of this process. Studies using this method with stem cells have been showing promising results for bone tissue engineering [27].

*3D-printing***:** 3D-printing is an additive manufacturing technique first portrayed in 1986. In this technique, thin layers of materials are deposited in a layered manner intermitted by hardening of the layers by ultraviolet (UV) radiation [28]. This method then developed to photopolymerization where mixed layers of a monomer gel and a photo-initiator agent are cured and crosslinked by a laser source according to the computer design [29]. This method offers many advantages like flexibility to use different powders and binders to tune various properties like mechanical strength, porosity, biocompatibility, etc. to generate scaffolds which can better mimic the ECM. In a study on bone regenerative scaffolds, pore sizes in the range of 20-50 μm were achieved [30]. An impediment drawback of 3D printing is the high temperatures used during the extrusion of polymer which would limit the use of proteins and cells because of their temperature-sensitivity [31]. Recent approaches using water soluble polymers and photo-crosslinking could solve this issue.

*Decellularization***:** Decellularization is a method which removes cells and debris from tissues and organs while preserving the biological activity, the biochemical composition and the 3-D organization and integrity of the native ECM [32]. As the decellularized the constructs are devoid of foreign cells, there is no significant chances of immune rejection [33]. Other than the use in tissue regeneration, it has also gained popularity in other fields like drug screening and stem cell differentiation studies. Different methods for decellularization include physical, chemical and enzymatic

treatments. After decellularization, the matrices can further be processed to generate injectable membranes, which can then be used as method for localized delivery with minimally invasive intervention [34]. Another simple but effective technique to enhance scaffold bioactivity is the deposition of solubilized ECM on the prefabricated scaffold surface. This allows the cells to interact directly with the ECM proteins which improves bioactivity along with achieving high mechanical properties [35].

*Electrospinning***:** This technique utilizes electric voltage to generate a 3D structure having fibers in the range of nanometers to micrometers with higher surface area [36]. Many natural and synthetic polymers have been used in this process like PCL, gelatin, collagen, polyvinyl alcohol (PVA), polycaprolactone (PCL), etc. [37]. A high DC voltage in the range of 10-40 kV is used to produce the fibers. Upon the application of such a high voltage, the polymer solution taken in the syringe becomes charged and the polymer droplet at the tip of syringe needle tend to move towards negatively charged/grounded collector as submicron fibers. Typical electrospun scaffolds show pore sizes in the range of 5-150 μm. To mimic native ECM, these scaffolds provide nano-scale fibrous structures having interconnected pores, and thereby showing great potential to fabricate functional tissues. The adaptability of this procedure, it`s non-obtrusive nature and temperature-independence are some of the advantages of this technique [38]. The ability to impart bioactivity in addition to structural features has led to the fabrication of scaffolds for tissue-specific functions [39]–[41].

2.2 Electrospinning for fibrous materials

Most of the ECM proteins have a fiber like architecture with diameters in the sub-micrometer range. For instance, collagens possess a fibrous structure in which the diameter varies from 50 - 500 nm. There have been many recent advances in the methods to develop ECM-mimetic nanofibrous materials. Nanofibrous materials have high

surface-to-volume ratio with regulated porosity and offer the flexibility to be made into a wide variety of sizes and shapes [42]. These unique features make the nanofibrous scaffolds promising for many biomedical and tissue engineering applications [43], [44].

Electrospinning and other related technologies like electro-spraying are some of the nanofabrication techniques that are used to generate nanofibrous microporous materials. The use of different polymers, their blends, or nanocomposites paves way for producing membranes of varied chemical compositions. These membranes are known for their great extent of processing flexibility which is helpful in optimizing their physical parameters such as fiber diameter, porosity, and pattern formation increasing demand for this supply. Electrospinning is one of the proven techniques to generate nanofibrous material that have a soldering-like attachment of the nanofibers at their intersections due to polymer chain entanglements and interpenetration after annealing [42], [45].

Nano-fibrous membranes have been found to adsorb higher serum proteins than less-porous macro -fibrous membranes [46]. Furthermore, other absorption analysis studies have revealed that the nano-fibrous scaffolds adsorbed larger amounts of fibronectin from serum in comparison to macro-porous scaffolds. These data indicate that the nano-fibrous scaffolds have better prospects of mimicking the natural ECM with enhanced tissue regeneration and which can also circumvent the potentially adverse immune reaction and possible chances of pathogen transmission when using naturally derived ECM based constructs (**Figure 1**).

Recent advances have made it possible to produce 3D nanofibrous scaffolds with the desired microstructure. In bioengineering, 3D scaffolds should bridge the gap between the nanofibrous technology and clinical applications [47]. There is also a great possibility of integrating bioactive molecules such as drugs, nanostructures and growth factors into fibers developed using various techniques. The high-loading capacity of

electrospun fibers make them promising materials for gene and drug delivery applications [48]–[51]. The therapeutic agents' encapsulation performance and bioactivity can be improved by carefully selecting materials and processing conditions [52]. Coaxial electrospinning is an advanced technique in which the fibers are in a core-shell form with complex microstructures produced using multiple pump system through coaxial nozzles. Many parameters influence the characteristics of the fibers such as the type of polymer, surface tension and viscosity of the solution, the polymer solution feed rate, needle-collector distance, needle tip size, *etc*. By precisely controlling these parameters it is possible to adjust the fiber diameter, porosity, and the nanofiber architecture [53].

Electrospun fibers offer several applications in tissue engineering such as vascular grafts [54], [55], nerve regeneration [56]–[58] and bone regeneration [59], [60]. They have been shown to enhance homeostasis, offer flexibility and mechanical strength, functionality when used as wound dressings [61]. A biologically inspired ocular repair dressing composed of membrane and electrospun fibers have been designed to treat corneal abrasions and ulcers on eye surfaces [62]–[64]. Zhou et al. extracted collagen from tilapia skin and generated electrospun ECM mimetic membranes based on it to expedite the rate of wound healing [65]. They also observed that scaffolds with biomimetic ECM structure and high specific surface area were more conducive to cell growth and stimulated human keratinocyte cell proliferation and epidermal differentiation. In other studies, collagen fibrils are mixed with other polymers as a traditional wound dressing so that the ECM mimetic structure would allow wound exudate absorption and moisture preservation which improves wound healing [66]–[69]. Sun et al. attempted to imitate the collagen`s basketweave pattern to generate ECM-mimetic microenvironment. Interestingly, the developed scaffolds provided higher fibroblast cell response during wound healing compared to random/aligned fibers [70]. In

addition, collagen fiber mats can resolve the issue of the higher trace of MMPs which deteriorate the human body's nonviable and viable collagen in chronic wounds [71]–[73]. Electrospun fibers have also been reported for use as sustained drug release systems for both transdermal delivery applications as well as for cancer therapy [74]. Overall, this technology has immense potential for researchers in the field of tissue regeneration. It offers the advantage of use of a variety of suitable polymers, polymer composites and polymer/inorganic composites with the flexibility to tune the microstructural properties and also have the capability to load bioactive molecules to combine therapeutic activity and tissue regeneration at the affected site [14]. ECM-inspired coating is a surface modification technique by which additional biological information can be incorporated [75]–[77]. A major step towards regenerative tissue implants is the accurate mimicking of the ECM making it possible to regulate the physical properties as well as the biological properties.

There are many advantages for electrospun fibers, such as polymer-dependent biodegradability and biocompatibility, relatively ECM-like mechanical properties, capability to load surface functional moieties and growth factors make it the most practical approach for the development of ECM mimetic membranes/scaffolds. Also, the high flexibility in choice of materials opens doors for delivering a wide variety of bioactive agents including proteins, antibiotics and anticancer drugs. The loading of drugs can be carried out by embedding, coating or encapsulation. A plethora of polymers, drugs and signaling molecules can be chosen to mimic the native tissues` structure and function [78]–[81]. The electrospun fibers have showed excellent capability for cell proliferation and differentiation both *in vitro* and *in vivo* [82], [83].

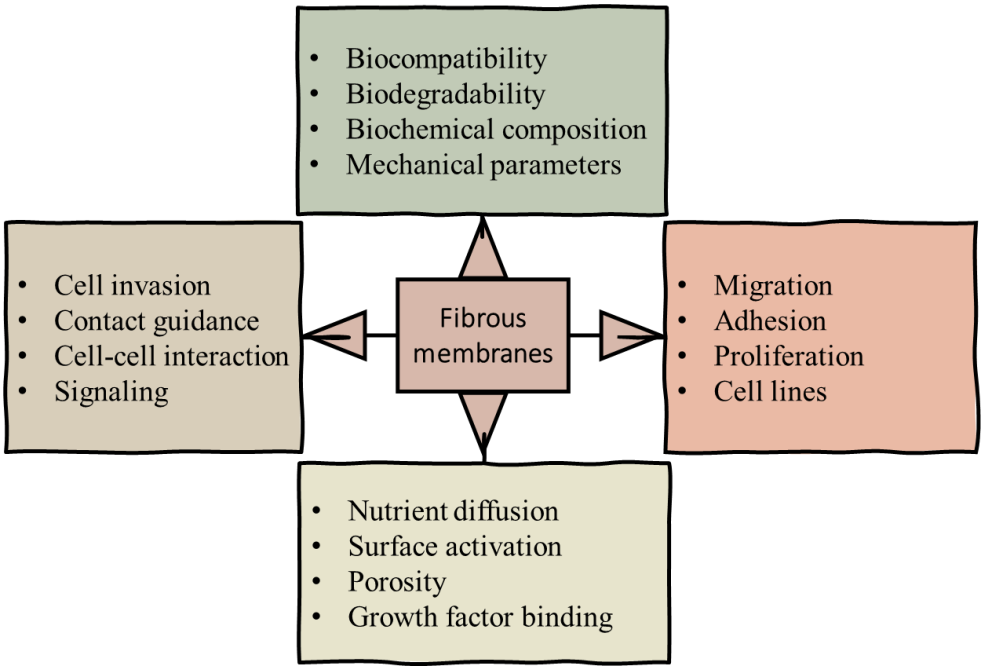

Figure 1. Desired properties in fibrous biomaterials for tissue engineering applications

2.3 Air-jet Spinning for fibrous membranes

Electrospun fibers have a distinct advantage over other tissue engineering materials in that they have a broad specific area and can integrate inorganic components on a nanoscale, making them perfect candidates for a variety of tissue engineering applications. The electrospinning process, however, is hindered by the slow rate of fiber processing and requires adequate conductivity to form a polymer jet. The need for a high voltage source raises the cost and complexity of the operation. While there are many ways to improve electrospinning's versatility, there is still a need for efficient methods to fabricate polymer–ceramic hybrid composites from microscale to submicroscale polymeric fibers. To overcome the limitations of this approach, a completely new strategy is needed. Air spray spinning is a low-cost option for spinning quickly and uniformly on a variety of substrates[84]. Air jet spinning is a quick and easy method for fabricating organic/inorganic hybrid nanocomposite membrane mats with highly interconnected porous structures. It does not necessitate a lot of expensive equipment and

has a low operating cost. It is entirely dependent on the use of pressurized gas dispensed at high speeds to stretch the polymer solution into thin fibers at the nozzle outlet, while the solvent begins to evaporate at the same time and continues to do so after the fibers are deposited onto a substrate. The air-jet is used in this technique to resolve the surface tension of the polymer solution and stretch it into ultrathin fibers while also vaporizing the solvent from the formed fibers due to the high speed of the air jet.

There are many factors that influence the spinning process. The distance of the collector from the tip of airbrush is one of the most important that influences the fibers. The polymer jet crystallizes at a particular distance from the nozzle exit forming fibers. This distance needs to be optimized to produce good fibers. If the distance is very close, bead formations are observed. The pressure of the air-jet used also influences the stretching of the polymer solution which affects fiber formation. The viscosity of the polymer solution is another important factor which influences the fiber formation by affecting the stretchability of the polymer jet.

2.4 PCL and PHBV polymers

Poly(e-caprolactone) (PCL) is the linear, semi-crystalline polyester derived from the e-caprolactone ring polymer opening. This polyester is organic and non-toxic and has excellent mechanical strength (**Figure 2(b)**). It is biodegradable and biocompatible. PCL is also market-oriented, provides a suitable cell adhesion, proliferation and differentiation environment, and supports ECM development. PCL is a very attractive tissue engineering biomaterial because of these physical and biological properties. PCL can be used to manufacture 3D structures suited to a variety of applications, such as skin, cartilage and vascular or heart tissue recovery by changing various processing techniques [85]–[87].

The PHBV microbial biopolymer is a safe natural material that is very promising for a wide range of applications due to its excellent inherent properties, such as

biodegradability and biocompatibility. On the other hand, many of its physical and mechanical properties are highly dependent on the 3HV material, making it unsuitable for some applications (**Figure 2(a)**). Using a variety of techniques outlined in this analysis, properties such as mechanical strength, water sorption and diffusion, electrical and/or thermal properties, antimicrobial activity, wettability, biological properties, and porosity can be enhanced to extend its potential applications. PHBV can be mixed with a variety of chemical materials to create advanced composites, including other polymers, natural fibers, carbon nanomaterials such as graphene and its derivatives, nanocellulose, nanoclays, and nanometals. In addition, this biodegradable polymer has excellent properties for producing porous scaffolds for tissue engineering [88].

Wound dressing materials made from polymer mixtures of synthetic and natural polymers have a synergetic effect and attractive injury curative benefits that individual polymers cannot achieve, according to recent studies. Shi et al. developed a new wound dressing that is antibacterial to the longest extent using the PCL-gelatin hybrid membrane that has electrospun quaternary ammonium salts [89]. Abdalkarim et al. developed the Electrospun PHBV/cellulose reinforced ZnO nanofibrous membranes for wound healing[90]. Daranarong et al. found that PHBV/PCL mixing scaffolds had less traction strength and an improved adhesion and proliferation efficiency of olfactory heating cells, compared to smooth PCL electrospun scaffolds[91].

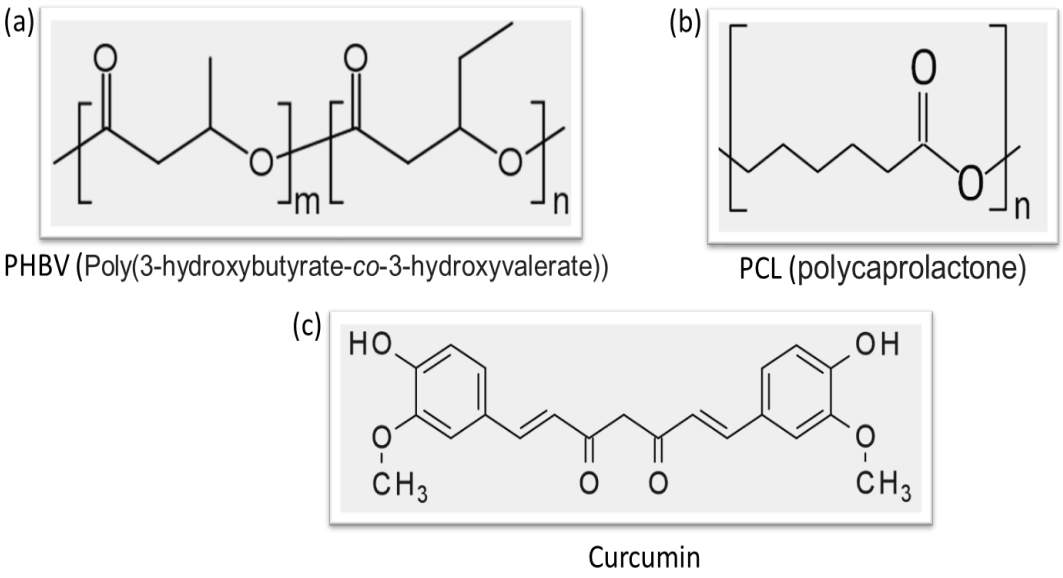

Figure 2. Chemical Structure of (a) PHBV, (b)PCL, (c) Curcumin

2.5 Curcumin as a wound healing agent

Curcumin or diferuloylmethane (1,7-bis(4-hydroxy-3-methoxyphenyl)-1,6-heptadiene-3,5- dione) and other curcuminoids are the key phytochemicals found in the Curcuma longa L. (Zingiberaceae family) rhizome known as turmeric (**Figure 2(c)**). This polyphenolic compound has been the focus of many researchers for various biological activities[92]. It is an ancient spice from Asia which is traditionally used for many ailments. There could be geographical variances in curcumin content among Curcuma species, due to hybridization with other curcumin-containing species. It has traditionally been used as an antimicrobial as well as an insect repellent. Several studies report that curcumin has broad-based antimicrobial, antiviral, and antifungal properties[93]. Because of the antimicrobial activity of curcumin's clinically proven long- and safe profile, various curcumin derivatives were developed for new antimicrobial agents. It was found to be particularly effective against fabrics.

Clinical studies have proven curcumin reduces superoxide radicals, hydroxy radicals and nitrogen dioxide to have healing properties in the granulation and

remodeling stages which are inhibited by oxidative stresses. To overcome this, researchers fabricated curcumin-loaded cellulose mats as wound dressing. The curcumin prevented the cell death that occurred in human fibroblasts due to hydrogen peroxide in the *in vitro* studies[94].

CHAPTER 3: MATERIALS AND METHODS

3.1 Materials

Sigma–Aldrich provided poly(e-caprolactone) (PCL, average Mn= 80,000; CAS No. 24980-41-4) and poly(3-hydroxybutyrate-co-3-hydroxyvalerate) (PHBV, natural origin, PHV content 12 mol%, Mn= 280,000, Mw= 690,000; CAS No.80181-31-3) (USA). Sigma-Aldrich provided curcumin powder, lipopolysaccharide (LPS), streptozotocin (STZ), xylazine, and ketamine (St Louis, MO, USA).

Chloroform (CHCl3) and phosphate buffered saline (PBS) were also purchased from VWR in the United Kingdom and used as obtained.

Gibco Technologies provided Dulbecco's modified Eagle's medium (DMEM), 0.2 % trypsin-EDTA (1X), phenol red, and phosphate buffered saline (PBS) pH 7.4 (10X). Sigma Aldrich provided eligible fetal bovine serum (FBS) of South American origin (sterile filtered) and dimethyl sulfoxide (DMSO).

3.2 Fabrication of PHBV/PCL membranes through air-jet spinning

To prepare air-jet spinning solutions, the PCL and PHBV were dissolved in chloroform, using a magnetic stirrer for 2 hours (1250 rpm) until a clear colorless solution was obtained. Different ratios of the PHBV/PCL were prepared (100% PHBV, 70/30 PHBV/PCL, 50/50 PHBV/PCL, 30/70 PHBV/PCL and 100% PCL) to find out the best composition that gave best properties for cell culture studies. The PHBV/PCL solution (15% [w/v]) was used for the formation of the fiber mats by air-jet spinning on a foil paper which was placed at 30 cm from the nozzle using a 4 bar pressure jet. For spinning, each solution was loaded into air-jet brush that has a stainless-steel flat needle tip of 0.4 mm inner diameter. The PHBV/PCL fibers were collected on aluminum foil-based collectors and were allowed to dry in open air for

about three hours so as to remove any remaining solvent. DSC results were used to confirm that the solvents was completely evaporated.

3.3 Fabrication of Curcumin-loaded PHBV/PCL membranes

The best composition from the previous study was used for incorporating curcumin to improve wound healing. Five set of samples were prepared for this study. The first set was named as blank PHBV/PCL without any loaded curcumin. However, in the other five sets CURCUMIN was added at concentrations of 0.5%, 1%, 2%, 3% and 5%. Each of these concentrations of curcumin were added to the blank PHBV/PCL polymer solution and was mixed with a magnetic stirrer for around 2 hours, until an orange-colored clear solution was obtained. For spinning, each solution was loaded into air-jet brush that has a stainless-steel flat needle tip of 0.4 mm inner diameter (**Figure 3**). The setup and parameters were same as mentioned in the previous section.

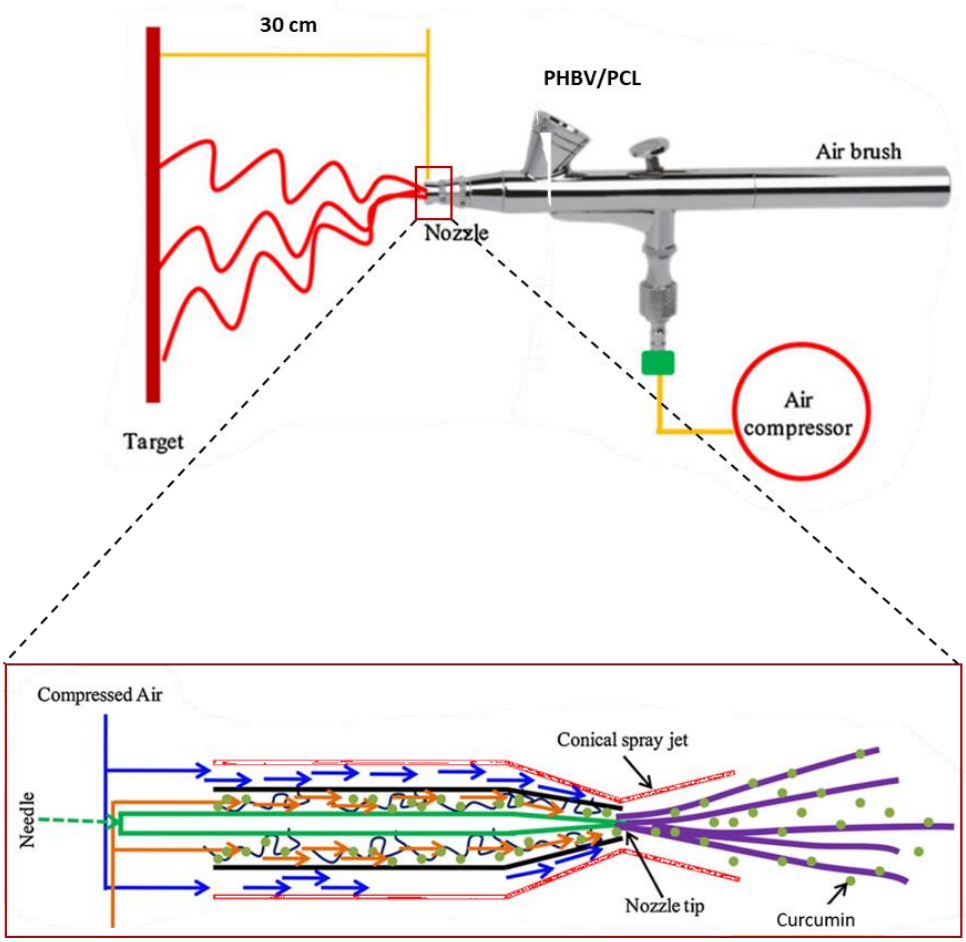

Figure 3. Schematic illustration of the steps involved in making CURCUMIN loaded PHBV/PCL membranes. Figure reproduced from [95] with permission from Elsevier.

3.4 Physical characterization

3.4.1 Scanning Electron Microscopy (SEM)

Using an FEI, Nova NanoSEM, 450 FE-SEM, the morphology and microstructure of the various membrane samples were determined using scanning electron microscopy (SEM). The fibers were cut into 1 cm^2 samples and double-sided adhesive tape was used to adhere them to the stubs. They were sputter coated with gold to a thickness of 200–500 microns to make them conductive. After loading the samples into the SEM, images were taken at different magnifications with a 20kV accelerating voltage. The average fiber diameter distribution was calculated using imagej software on a sample size of 100 fiber diameters.

3.4.2 Fourier Transform Infrared Spectroscopy (FTIR) of the membranes

FTIR spectroscopy was used to determine the chemical composition of PHBV/PCL and curcumin-loaded PHBV/PCL samples. The spectra were determined using various samples of PHBV/PCL and curcumin-loaded PHBV/PCL. On a PerkinElmer (USA) FTIR Spectrum 400, the absorbance peaks of FTIR were measured. The spectra were measured in the 400-4000 cm^{-1} frequency range. At room temperature, it was registered with a resolution of 4 cm^{-1} and a scanning frequency of 32 times [42].

3.4.3 Differential Scanning Calorimetry

Differential scanning calorimetry (DSC) was used to determine the crystallinity and melting temperature of the various samples, and data was collected using PerkinElmer, Jade, USA equipment. Thermal analysis of pure PCL, pure PHBV, blank PHBV/PCL, and PHBV/PCL membranes filled with different concentrations of CURCUMIN was carried out at a rate of 10^{o}C/min from room temperature to 300^{o}C. Samples weighing at least 10 mg were weighed and sealed in aluminum crucibles. Following that, the weighted crucibles were placed next to the reference cell, and the measurements were taken.

The heating scan yielded the melting temperature (Tm) and enthalpy of fusion (ΔHm), while the cooling scan yielded the crystallization temperature (Tc) and enthalpy of crystallization (ΔHc). The melting enthalpies (ΔHm) of PCL and PHBV were used to measure the crystallinity degree:

$$Xpol = \Delta Hpol\,/(\Delta H0pol * \mu)$$

Where the superscript pol refers to PHBV or PCL, μ is the weight fraction of the considered polymer and ΔH^{0pol} is the melting enthalpies of fully crystalline polymers, 109 J/g for PHBV and 139.5 J/g for PCL.

The crystallinity of the fabricated samples greatly influences the degradation behavior. It also affects the release of drugs incorporated into the polymer matrix.

3.4.4 Thermogravimetric Analyzer (TGA)

The thermogravimetric analyzer (TGA) was used to investigate the thermal degradation activity of the different membranes (PerkinElmer, Pyris 6, USA). It looks at the weight loss over time as the temperature increases. A purge of N2 was used to heat 20 mg of the sample from room temperature to 700^{o}C at a heating rate and flow rate of 5 ^{o}C/min and 70 ml/min, respectively. These results provide insight into the behavior by which the polymer degrades and releases the incorporated active agents which in turn affects the wound healing activity.

3.4.5 X-Ray Diffraction (XRD) Patterns

X-ray diffraction (XRD) was used to examine the crystalline structure of pure PCL, PHBV, various compositions of PHBV/PCL, and PHBV/PCL membranes filled with CURCUMIN using an Empyrean, Malvern Panalytical XRD method. The 10mg membrane samples were weighted and put in the XRD specimen holder. The scanning range of 2 was 0° to 60°, with a voltage of 40 kV and a current of 30 mA. The scanning scope of 2 was ranged from 0° to 60°, voltage was 40 kV, and current was 30 mA. The initialization was started at room temperature with a scanning rate of 5°/min to 118^{o} with a phase size of 0.032^{o}, scanning scope of 2 was ranged from 0° to 60°, voltage was 40 kV, and current was 30 mA.

3.4.6 Swelling Properties of the Samples

The gravimetric technique was used to investigate the swelling properties of pure PCL, pure PHBV and PHBV/PCL membranes filled with CURCUMIN. Before being placed in a petri dish with distilled water, the dried samples were measured (DW). In

a temperature-controlled water bath, the petri dishes were then held at room temperature. The weight of swollen membrane samples was later measured using a Mettler Toledo digital balance after precise time intervals. By extracting the swollen membrane from water and then drying it with filter paper to remove excess water, the weight of the membrane was calculated.

For the purposes of calculating the statistical average and standard deviation, samples were replicated three times. Where wf is the membrane's weight after being submerged in water. On the other hand, wi is the weight of dry samples until they are submerged in water.

$$Swelling\ ratio\ = (wf - wi)/wi$$

3.4.7 Mechanical Performance of air-jet spun Samples

The mechanical properties of the fabricated samples influence the ability of the scaffolds to absorb and hold the exudates without collapsing at the wound site. This study was also done to assess how the blending of the two polymers affected the mechanical behavior of samples. The natural skin of human beings has varying mechanical properties depending on many factors like age, part of the body, etc. The mean tensile strength is in the range of 27.2±9.3MPa, the mean elastic modulus was 98.97±97 MPa [96]. The tensile strength of blank PHBV/PCL membrane samples was tested using a Lloyd Instruments LR50K Plus Tensile Testing Machine. The membrane was cut into a dog-bone shape with a height of 30 mm and a length of 10 mm, and then inserted in the tensile tester's jaw. At room temperature (23°C), the equipment was set to run at a speed of 10 mm/min. The thickness was measured using a digital vernier caliper. The membranes' strength was then assessed before the samples were broken down. For the measurement of mean and standard deviation, the tensile strength was measured five times.

3.5. In Vitro Cell Studies

To determine the cell adhesion and proliferation on the PHBV/PCL membranes, Crystal Violet staining was carried out. To determine the cytotoxicity and viability of Curcumin releasing membranes, scratch assay and MTT assay were performed.

3.5.1 Cell Proliferation and Viability study

The MTT [3-(4,5-Dimethylthiazol-2-yl)-2,5-Diphenyltetrazolium Bromide] colorimetric assay was used to assess cell proliferation and viability using treatments of blank PCL-PHBV and PHBV/PCL filled with CURCUMIN membranes.

*MTT Assay***:** The protocol was adopted from previous literature on similar scaffolds [97]. 3T3 fibroblast cells were seeded at 40,000 cells in each well of a Corning 12-well plate overnight to determine metabolic activity, and samples of membranes consisting of blank PCL-PHBV, PHBV/PCL loaded with CURCUMIN were placed in respective wells of the 12-well Corning plate. After 1 day of incubation at 37°C with 5% CO_2 humidification, the MTT assay was performed. During the MTT assay, the cell culture media was replaced with fresh media, and the membrane samples were extracted from their respective wells of the Corning 12-well plate. The cells were stained by adding 100 µl of MTT dye solution to them and incubating them at 37ºC for 3 hours. After that, 300 µl of DMSO solution was applied to dissolve the formazan crystals, and the plates were shaken for 10 minutes to boost the results. Finally, 100 µl of this was transferred to 96 well plates, and absorbance was measured at 570 nm using a TECAN infinite F200 PRO microplate reader (Tecan Austria GmbH). Using the formula proposed in the previous literature [98], the absorbance was transformed to % cell viability:

$$(\%\, Cell\ viability) = [100 \times (sample\ absorbance)/(control\ absorbance)]$$

The results of the experiment were presented as means of triplicates with standard

deviations.

3.5.2 Cell Migration by Scratch Assay

A wound scratch assay was used to determine the effect of Curcumin released from membrane samples containing blank PCL-PHBV and PHBV/PCL loaded with CURCUMIN on the migration of 3T3 fibroblast cells. Overnight, 3T3 cells were seeded in a Corning 12 well plate at a concentration of 40,000 cells/ml. When the cells had reached 90% confluence, a straight scratch line was made with a 100 µL tip. The debris of cells flowing in the medium was removed by aspirating it and washing it three times with sterile 1X PBS. The 3T3 fibroblasts were given 5mg of membrane samples and incubated for 24 hours at 37°C with a humidified CO_2 pressure of 5%. The migration of cells was observed after 24 hours and photographs were taken with an Olympus X53 microscope. Following that, the migration distance was calculated using Image J software. With means and standard deviations, the experiment was recorded in triplicate.

The cell migration was calculated by the following formula:

$$Wound\ contraction\ (\%) = \frac{Ai - Af}{Ai} * 100$$

where A_i is initial scratched area at 0 hours and A_f is the healed area aster 24 hours of incubation with the samples.

3.5.3 Cell adhesion by crystal violet assay

Prior to UV sterilization of fibers for 1 hour, the adhesion of 3T3 cells on PHBV/PCL samples and curcumin integrated PHBV/PCL scaffolds was examined. The fabricated fibers collected on the 18 mm round glass cover slips were seeded with 3T3 cells (4 104 cells/cm2) in a 24-well plate and allowed to adhere for 4 hours. The extent of 3T3 cell adherence was determined using the crystal violet assay. As a control, TCP

(Tissue Culture Plate) was used. The cells were then incubated for 4 hours at 37°C in a humidified atmosphere containing 5% CO_2. The 3T3 cells were then washed with 1 PBS (phosphate buffered saline) to remove any unattached or weakly attached cells. The remaining cells were then fixed for 20 minutes with 4% paraformaldehyde. For 10 minutes, fully attached cells were stained with crystal violet (0.1 % (w/v)) in ethanol (10%). The crystal violet stain was extracted from the cells by washing them in PBS. Finally, an Olympus X53 microscope was used to photograph the adhered 3T3 cells on the membranes.

3.6 Statistical Analysis

Means and standard deviations were used to interpret the data first (SD). All of the experiments were carried out three to four times in a row. Using SPSS statistical tools, all samples were statistically analyzed using the t-test in Origin statistical software. The confidence interval was taken as 5% to check the significantly different results ($p<0.05$).

CHAPTER 4: RESULTS & DISCUSSIONS

Membrane samples were initially characterized by SEM, FTIR, XRD, TGA, DSC, swelling behavior, tensile strength, and later biologically by In vitro assays such as cell viability assay (MTT assay), and cell migration (scratch) assays. A detailed description of results of each parameter are described in detail below.

4.1 Finding the PCL\PHBV optimum composition

4.1.1 Physical Characterization

SEM

In air-jet spun nonwoven mats, SEM was used to study the bead and defect-free morphology of fibers with average diameter, interconnected pores structures. The air-jet spinning method was obviously efficient because all of the fibers were cylindrical, continuous, and defect-free. As shown in the figure, the SEM micrographs of the air-jet spun PHBV/PCL membranes show a uniform fiber diameter distribution without any beads. Figure 4 and Table 1 indicate the FESEM micrographs and diameters of all the different fibers, respectively. Pure PCL fibers tended to be thinner and more uniform than pure PHBV fibers in general. All of the PHBV/PCL fibers were made with a concentration of 15 % (w/v) chloroform, as previously mentioned. PHBV's molecular weight (400–600 kg mol/1) was also higher than PCL's (80 kDa), resulting in the development of much larger, random, and non-uniform PHBV fibers.

All samples consisted of randomly arranged, defect-free fibers with a smooth, bead-free surface (**Figure 4**). The mean fiber diameter for all samples showed a decreasing trend: 0.99±05μm, 0.55±0.25μm, 0.43±0.41μm (PHBV/PCL 50/50), 0.19±0.1μm (PHBV/PCL 30/70), 0.32±0.13μm and 0.32±0.13μm (PCL). The air-jet spinning technology is a quick process that produces a small volume of a polymeric solution

(the jet emerging from the nozzle) that is constantly subject to rolling instability and solvent evaporation as it travels from the nozzle to the target. When the solvent concentration falls below critical levels at a certain pressure, the beginning of a glass transition and/or crystallization controls the fiber forming mechanism [19].

Table 1. Fiber diameter distribution of PHBV/PCL membranes sample

Composition	Mean (µm)	S.D	Minimum (µm)	Median (µm)	Maximum (µm)
100% PCL	0.19	0.10	0.04	0.18	0.57
PHBV/PCL 30/70	0.32	0.13	0.12	0.31	0.87
PHBV/PCL 50/50	0.52	0.41	0.15	0.47	2.75
PHBV/PCL 70/30	0.55	0.24	0.21	0.52	1.63
100% PHBV	0.99	0.5368	0.22	0.93	3.70

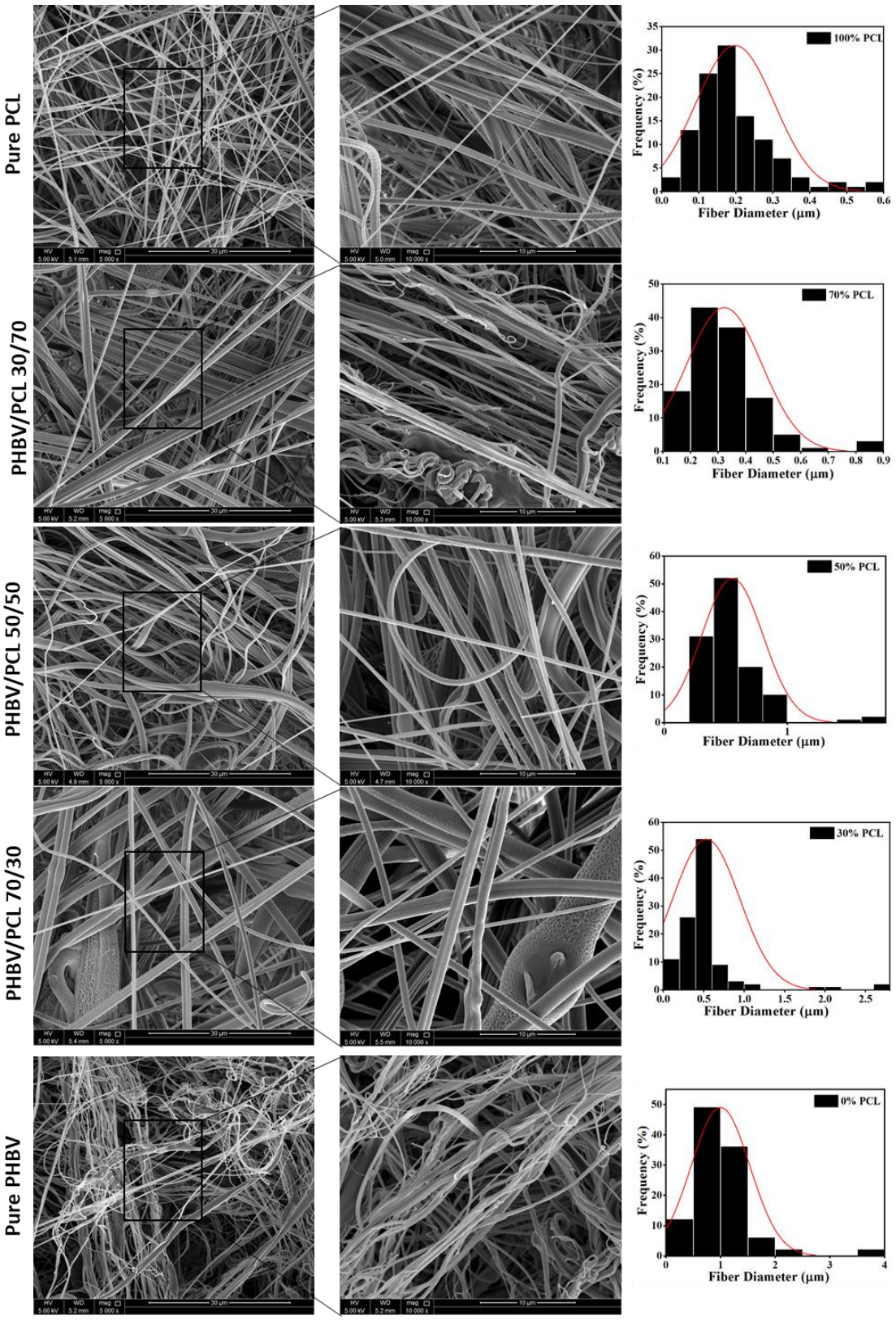

Figure 4. SEM micrographs of air-jet spun mats: Pure PCL, PHBV/PCL 30/70, PHBV/PCL 50/50, PHBV/PCL 30/70 and Pure PHBV. The fiber diameter distribution curves are also attached alongside the micrographs

XRD

Figure 5 shows registered XRD spectra for air-jet spun mats. In all cases, the PCL portion must be linked to the two key peaks. The main PCL peaks are found at 2θ = 21.3 and 23.7, which correspond to the (110) and (200) planes, respectively. Due to the peculiar characteristics of poly(hydroxybutyrate) (PHB) and poly(hydroxyvalerate) (PHV), PHBV exhibits isodimorphism, as previously stated (PHV). The crystalline structure was determined by the HV material, with PHBV crystallizing in the PHB lattice for HV in the range of 0–29mol %. According to Wang et al., a major polymeric chains orientation is likely to occur at the nozzle's entry, where the jet is stretched severely. The absence of sharp peaks in the PHBV sample indicates that the large peaks correspond to the amorphous structure. As the concentration of PCL in the PHBV/PCL scaffolds is increased, the peaks of PCL appear to become more visible. This also confirms our suspicion that the blend is properly blended, as shown by the SEM photographs. XRD spectra of air-jet spun PHBV/PCL blends showed the characteristic patterns in the used measurement conditions, with no noticeable peak change with respect to the tidy components. The crystallinity/amorphous of the polymer components in the blends will affect the degradation of the fibrous mats during wound healing. More amorphous nature helps to accelerate the degradation of the material, as observed in the literature. The blending has resulted in the decrease of intensity of crystalline peaks with increasing content of amorphous PHBV. This shows that the blending will decrease the degradation time required by the pure PCL, which is helpful for the potential use as biodegradable wound dressing materials.

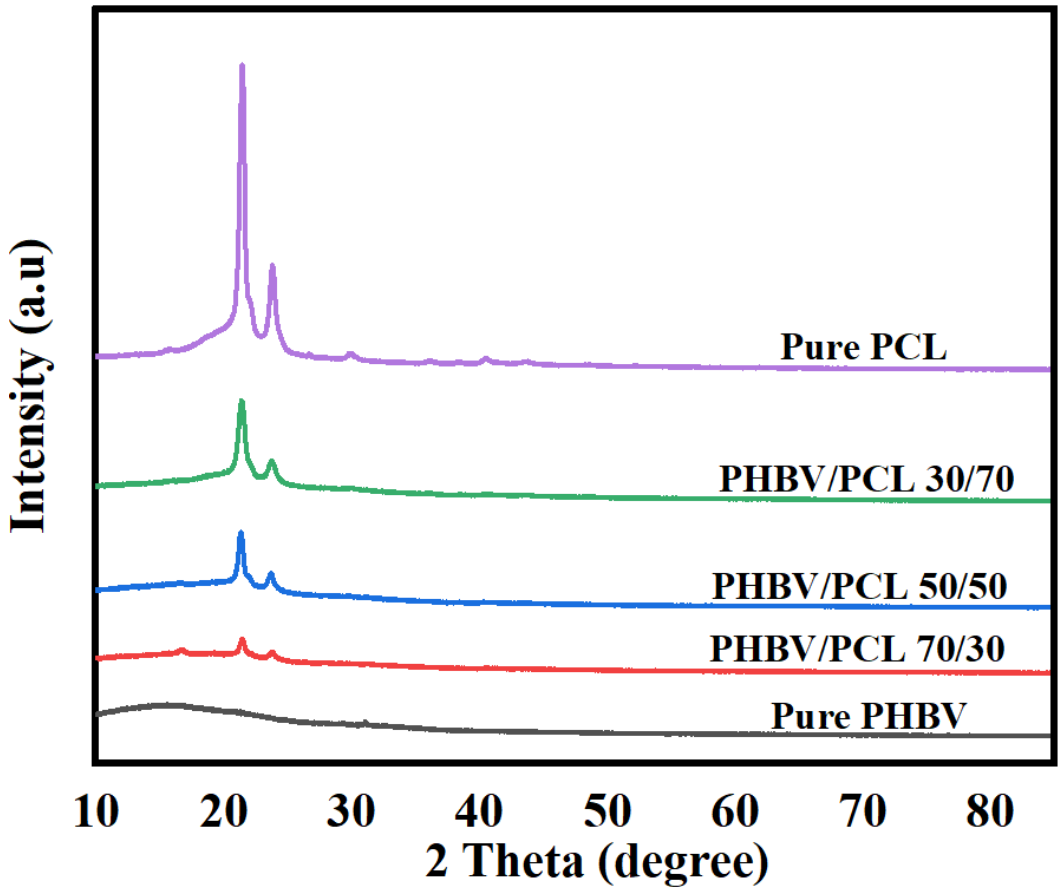

Figure 5. XRD spectra of all PHBV/PCL blended samples to assess the nature of the blended components in the fibers.

FTIR

All of the scaffolds in the study had their spectra analyzed and compared to pure PHBV and pure PCL spectra. For PCL scaffolds, the FTIR spectra revealed many distinct bands at 1751 cm^{-1} (C=O stretching), 1353 cm^{-1} (C-O and C-C stretching), 1240 cm^{-1} (C-O-C asymmetric stretching), 1175 cm^{-1} (OC-O stretching), and 1155 cm^{-1} (C-O-C symmetric stretching). Both samples had chemical functional groups that were very similar, according to the results obtained for PHBV/PCL composite scaffolds. The absorption peaks of PHBV were observed at 1740 cm^{-1} (C = O stretching), 1266–1472 cm^{-1} (C-H stretching), 1232 cm^{-1} and 1124 cm^{-1} (C-O-C stretching), 1170 cm^{-1} (C-O asymmetric stretching), and 1058 cm^{-1} (C-O symmetric

stretching). Figure 6 depicts the infrared spectra and main absorption bands of different samples. The FTIR spectra of PCL and PHBV matched those seen in the literature. The transmission peaks of fibers made using various methods are close to those of pure PCL and PHBV, and no new absorption peaks have emerged. These findings revealed that there was no chemical bond between polymers during the fiber preparation process, indicating that it is safe to assume that the initial components were not chemically changed. Therefore, it is safe to assume that the blended materials will not impart any toxicity to the mats.

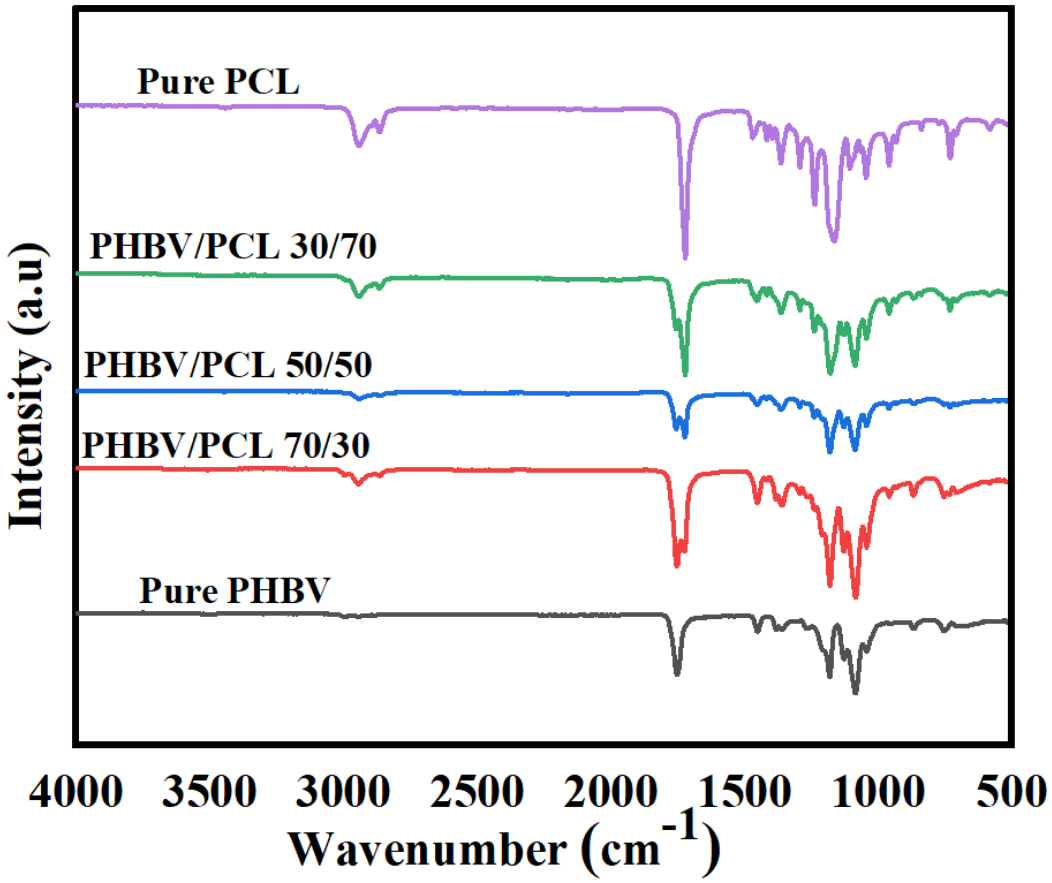

Figure 6. FTIR spectra of all PHBV/PCL blended samples to check the formation of chemical bonds between the blended polymers

DSC

The thermal properties of air jet spun samples are summarized in Table 2, while DSC

thermogram is shown in Figure 7. The PHBV and PCL melting temperatures were approximately 155 °C and 69 °C. The melting of primary crystallite material and the melting of re-crystallized material had previously been due to PHBV's double melting point. In the range of 140–155 ^{o}C, a double fusion peak was detected for PHBV/PCL fusion, and about 60 ^{o}C were detected for a single peak. The endotherms were used to measure the degree of crystallinity. The crystallinity of the PHBV component was close to that of the neat polymer in all compositions (i.e., about 40 %). The degree of crystallinity of the PCL part increased over time, with PHBV/PCL 50/50 hitting a peak crystallinity of around 50%. This finding supports the previous microstructure discussion, which leads to the conclusion that the increase in PCL helped to influence the relative mechanism of PHBV crystallization.

In line with the previous XRD results, this result indicates that the polymer blend is made up of two immiscible components. Given that molecular chains must be rearranged in small fluid volumes, these results indicate that the two polyesters interacted with the nucleation and growth of crystalline structures during air-jet spinning, allowing for more effective grid lattice organization. In addition, it is obvious that Tc (PHBV) in blends decreased for air-jet spun mats by about 11°C compared to a neat PHBV when comparing the thermal data in Tables 2. Because of the heterogeneity deactivation, these results suggest that the two immiscible polyesters interacted in some way in the nucleation and creation of the crystalline domains. Incredible binary combinations' crystallization behavior is well known to be highly dependent on the stage before crystallization. Based on the preceding discussion, the presence of crystalline PCL fields can be deduced to improve the crystallization of PHBV. Sample microstructure were affected by various solvent evaporation rates and stresses induced in the polymer solution when air throttle was

spinning. Also, as discussed in XRD, the change in crystallinity of the polymers in the blends will improve the degradation behavior which is required for quicker degradation time.

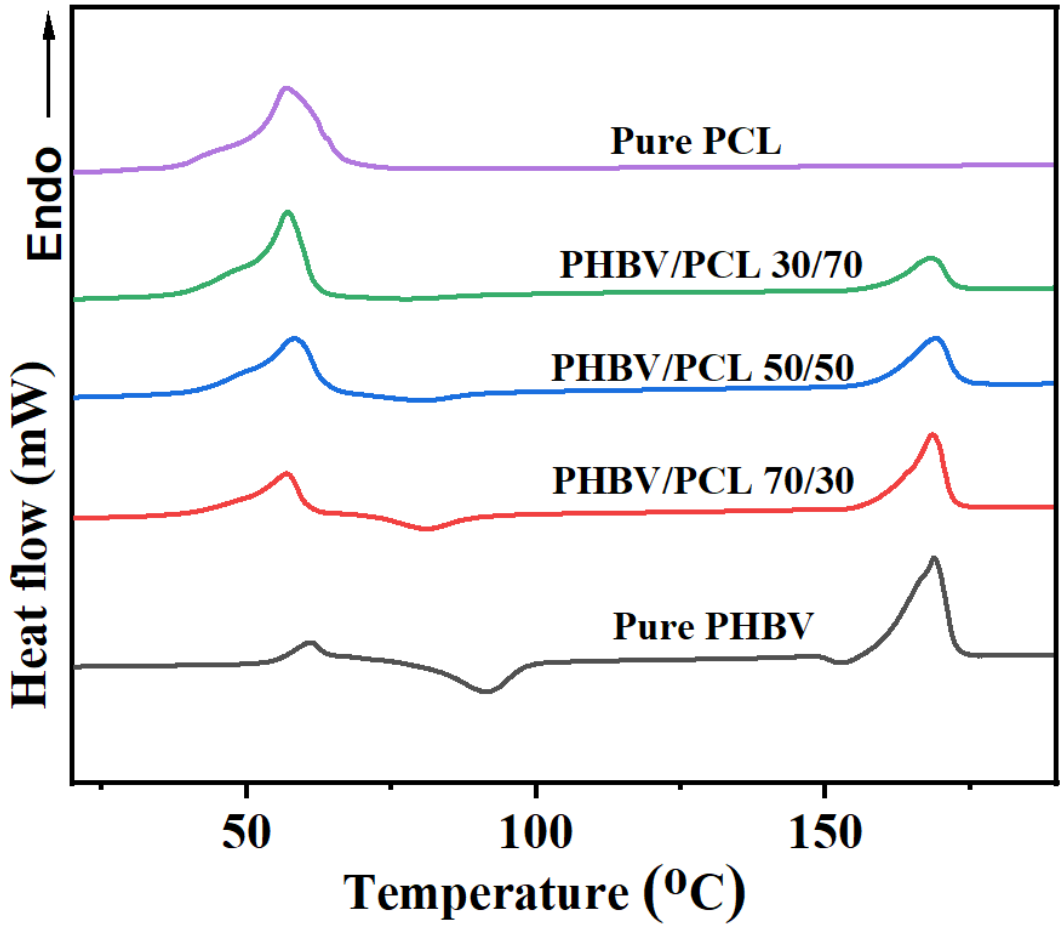

Figure 7. DSC heating thermogram of all PHBV/PCL air-jet spun mats to analyze the crystalline content in the blends which affects the mechanical behaviour as well as degradation behavior of the samples.

Table 2. DSC parameters for PHBV/PCL membrane samples. T_c is crystallization temperature from cooling pass, T_m is melting temperature from the heating pass and X is the crystallinity % of the specific polymer

Sample	PHBV			PCL		
	Tc(°C)	Tm (°C)	X (%)	Tc(°C)	Tm (°C)	X (%)
Pure PCL	-	-	-	28	54.5	39.7
PHBV/PCL 30/70	-	167.7	47.0	25.2	54.2	37.7
PHBV/PCL 50/50	-	167.5	42.9	27.2	54.3	37.1
PHBV/PCL 70/30	96.5	166.7	43.4	25.2	53.6	31.7
Pure PHBV	99.5	167.8	41.3	-	-	-

TGA

Thermal stability is a significant consideration in PHBV blend research and applications. TGA was used to investigate the blends' thermal degradation kinetics, as shown in Figure 8. Pure PHBV and PCL degradation begins at approximately 265 and 348 °C, respectively, and is completed at 346 and 440 °C, respectively, in a single step. The weight loss of PHBV/PCL is two-step, as shown by the TG curves of the blend samples, with initial and final decomposition temperatures close to those of pure PHBV and PCL. As a result, the TGA findings in this analysis are close to changes in PHBV/PCL blends previously recorded [99]. This study confirms that there was no unstable behavior shown by the blends in their thermal degradation. This

is in conformity with the results from the DSC results where it was observed that the two polymers in the blends existed as immiscible components. Within the range that a human sin usually exposed to (upto a maximum of 55 ^{0}C in peak summer under direct sunlight), there does not seem any erratic degradation behavior.

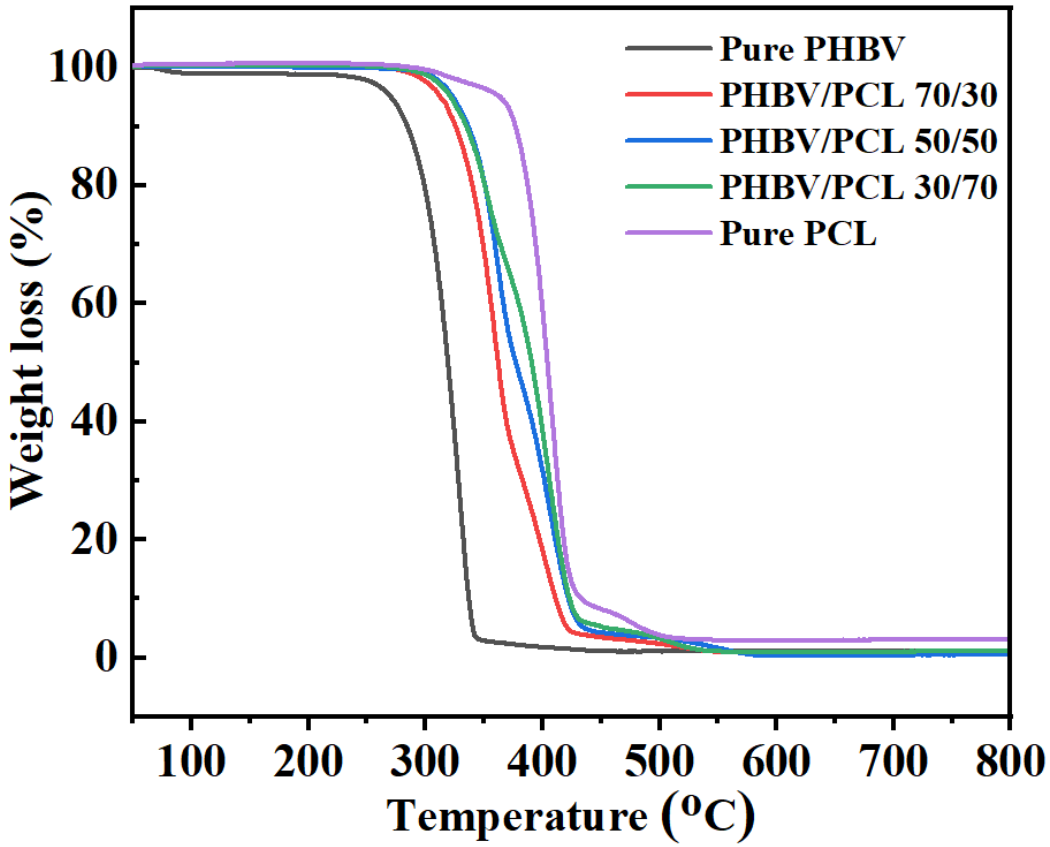

Figure 8. TGA of different PHBV/PCL blends to analyze the thermal degradation behavior of the blends

Water retention study

Swelling experiments are preliminary tests for determining if biodegradable polymers are compatible. The fibrous scaffolds' ability to absorb vast amounts of water and swell as a result makes them a good choice for use in living tissues, giving them unique physical properties [100]. The water uptake of samples was investigated using

the swelling capability of prepared fibers. Swelling ability and water absorption properties, which suggest hydrophilicity potential in three dimensions, are not the same as surface hydrophilicity. In numerous studies, highly swelling matrices have been shown to benefit cell attachment, growth, and internal migration into three-dimensional scaffolds. The higher the value of the swelling ratio, the better it is for wound dressing applications as it allows for more exudate removal from the wound site.

Figure 9 shows the water absorption capacities of pure PCL, pure PHBV, and PHBV/PCL scaffolds in 0.1 m PBS at room temperature after 3 days. For PHBV/PCL 70/30 scaffolds with a maximum swelling ratio of around 15, the water absorption rate increased steadily in the early 8 h and rapidly in 4 d. Over the course of four days, the water absorption rate of PHBV/PCL blends increased steadily, reaching a swelling ratio of around ten. The water absorption capacities of PHBV scaffolds were lower than the water absorption capacities of PCL scaffolds at any given time point. At 4 days, the water absorption capacities of PHBV scaffolds were lower than those of PHBV/PCL blends and PCL scaffolds. As PHBV was blended into PCL scaffolds, the porosity of the scaffolds decreased, as did the water absorption capacity of the scaffolds. Surface wettability has been shown to be influenced by both micro- and nanoscale roughness. It's possible that it had an effect on water absorption properties.

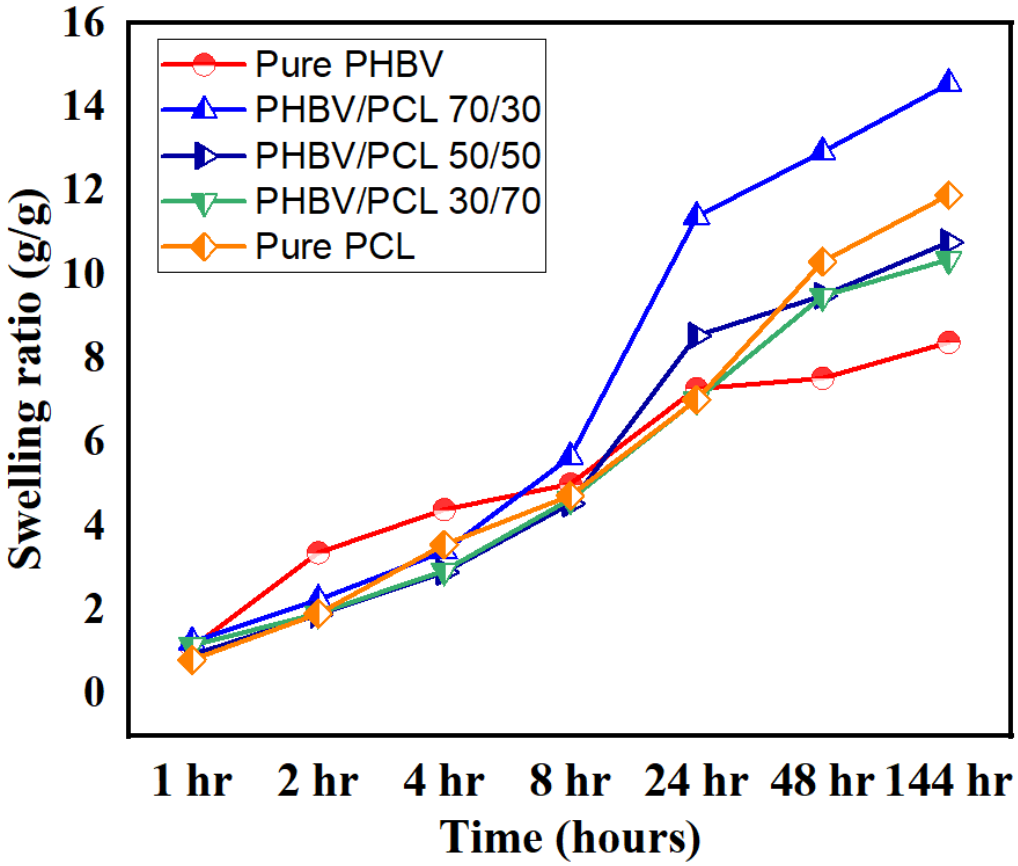

Figure 9. Water retention capacity of various blends of PHBV/PCL in terms of swelling ratio. The values of the swelling ratios are taken as averages of three sample sets of each blend.

Mechanical strength study

The stress-strain plot of all the samples was obtained from the testing machine. Table 3 shows the mechanical properties of air-jet spun mats. Among the polymers, PCL had the highest tensile strength and the largest deformation at break. The results showed a steady improvement in tensile strength and elongation at split as the PCL content in PHBV/PCL blends was increased. The initial linear stress–strain action of air-jet spun mats is governed by fiber packing density in general. The higher the fiber packing density, the better the air-jet spun material contrasts the reorienting power, since non-woven fibers reorient along the load direction. A second stage occurs as the

loading is increased, powered by fiber mechanics, which is determined by polymer chemistry and fiber dimension. It was difficult to set up pure PHBV samples for testing on the machine because they were extremely fragile.

The engineering stress-strain curves are shown in Figure 10. The increase in PCL in the chemical composition usually increases the strength, while plasticity was affected by the PHBV content of mixtures. However, of all membranes tested at this strain rate, PHBV/PCL 50/50 showed the best combination of strength and plasticity, and could be used in biomedical applications where swelling improves water uptake and thus cell proliferation. The PHBV/PCL 50/50 tensile strength and plasticity were up approximately 0.7 MPa and 100 % in comparison to pure PHBV. In the literature, PCL has been combined with various bio-polymers to produce more advantageous nano-scaffolds and PCL membranes are presented in line with previous studies for improved mechanical properties. In addition, the PHBV/PCL membrane Young`s modulus was usually linearly proportional to the membrane PCL in 50% of the PCL, but the Young`s modulus decreased with the increasing of the PCL composition. The mean tensile strength of human skin is in the range of 27.2±9.3MPa while the mean elastic modulus is 98.97±97 MPa [96]. The results of this study is nowhere close to these numbers but is comparably close to similar polymer blend studies using electrospinning process [101]. Compared to electrospun mats of similar blend composition, the air-jet spun mats have reached 50% of the strength.

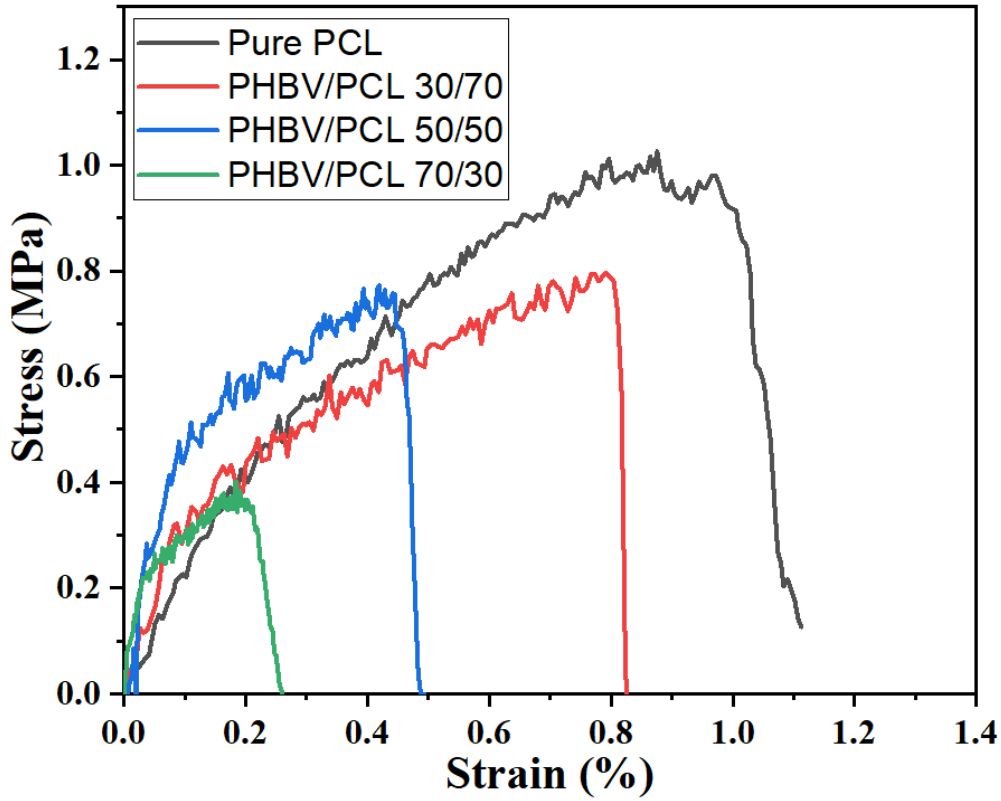

Figure 10. Tensile stress-strain curves of different blends of PHBV/PCL composite scaffolds

Table 3. Mechanical properties of air-jet spun PHBV/PCL composite membranes

Samples	Maximum elongation (%)	Ultimate tensile strength (MPa)	Young`s modulus (MPa)
Pure PCL	102 ± 5.3	1.03 ± 0.13	2.06 ± 0.4
PHBV/PCL 30/70	83 ± 5.8	0.82 ± 0.17	3.04 ± 0.8
PHBV/PCL 50/50	48 ± 4.6	0.79 ± 0.15	5.5 ± 0.6
PHBV/PCL 70/30	24 ± 3.9	0.41 ± 0.18	6.02 ± 0.5
Pure PHBV	-	-	-

4.1.2 *In Vitro* cell studies

At 3 and 7 days after cell culture, the proliferation of 3T3 fibroblast cells cultured on each PHBV/PCL blended scaffold was assessed. The number of cells cultured on each scaffold increased as the cultivation period went on, as shown in Figure 11. Overall, the cell proliferation rate increased as the amount of PHBV blended into the scaffolds increased; large increases in the number of cells were observed on all composite PHBV/PCL scaffolds after a 7-day culture cycle, compared to pure PCL scaffolds. The introduction of PHBV into the PCL scaffold aided cell adhesion first, and then stimulated cell proliferation. These findings appeared to corroborate previous findings that PHBV could enhance cellular functions. Cell morphology and interactions between cells and scaffolds can be studied using these photos. The majority of cells began binding to the fibers over the scaffolds three days after seeding. At any given time point, the most expansion occurred on the surface of the PHBV/PCL 70/30 scaffold. The adhesion and proliferation of the PHBV/PCL 50/50 is comparable to the PHBV/PCL 70/30. Although the pure PHBV fibers had the best adhesion, the random orientation and disconnected fibers prevented better proliferation, as shown in the figure. When compared to other scaffolds, the water absorption capacities of the PHBV/PCL 70/30 scaffold were also the largest, indicating that the wettability of the substrate plays an important role in mediating cell activity.

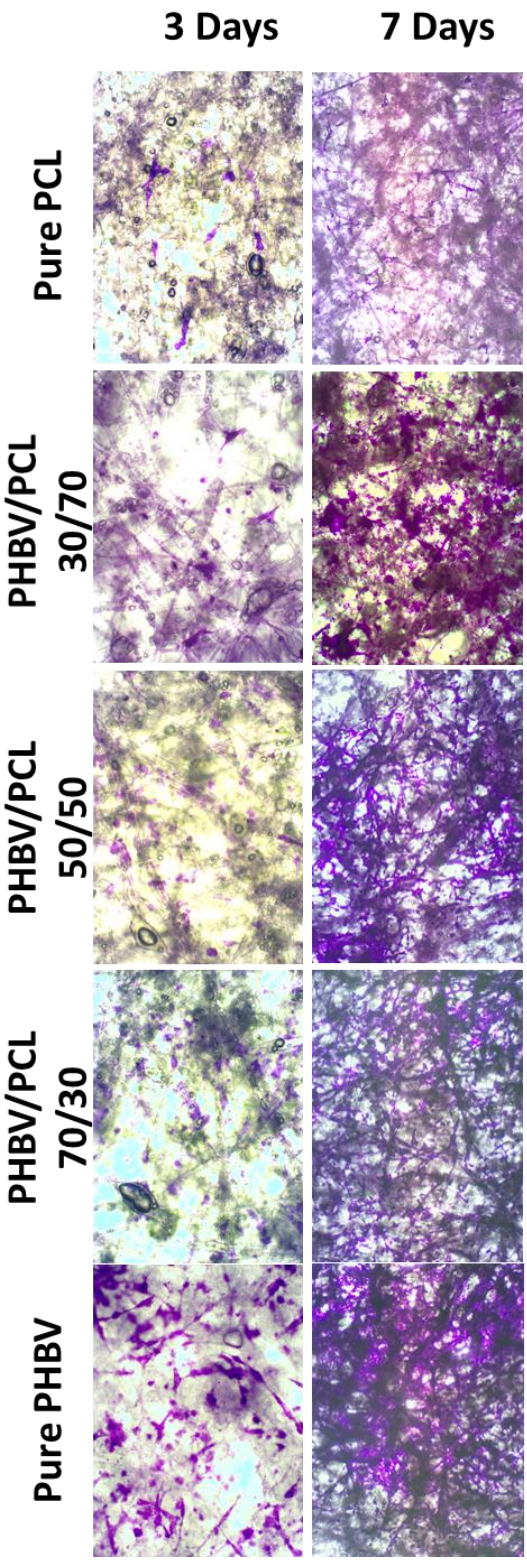

Figure 11. Adhesion of 3T3 fibroblast cells to the different compositions of PHBV/PCL scaffolds after 3 days and 7 days of culture

4.1.3 Inferences

SEM results showed that the fiber diameter increased with increasing PHBV content. Thermal analysis and spectral analysis showed that the blending influenced the crystallinity of the polymers and that they existed as immiscible components in the blends. Tensile strength study showed that the strength increased with increasing PCL content. For PHBV/PCL 50/50, the strength was around 75% of that of pure PCL. Cell culture study showed that the increasing PHBV content increased cell adhesion and proliferation. The adhesion and proliferation of the PHBV/PCL 50/50 is comparable to the PHBV/PCL 70/30. From the water retention study, tensile strength study and cell adhesion study, it can be inferred from the above observations that PHBV/PCL 50/50 can provide the best possible combination of mechanical and biological properties suitable for wound dressing applications.

4.2 Incorporation of curcumin into PHBV/PCL samples

4.2.1 Physical Characterization

SEM

In this analysis, we used different curcumin concentrations of 0.5, 1, 2, 3, and 5 (% w/w) to prepare PHBV/PCL air-jet spun fibers. Image J was also used to measure fiber diameters (**Table 4**). To fabricate smooth and uniform fibers, various parameters from the previous study were used, such as polymer concentration and air-jet spinning parameters. SEM images show that air-jet spinning produced smooth and uniform nanofibrous structures (**Figure 12**). The average diameter of PHBV/PCL blank fibers was 0.497±0.3 μm. The average diameter of the 0.5, 1, 2, 3, and 5 % loaded fibers increased to 0.912±0.3 μm, 0.53 ±0.4 μm, 0.81±0.4 μm, 0.86±0.3 μm, and 1.2±0.5 μm, respectively, when curcumin was added. The addition of curcumin to the solution

increased the density and may have resulted in a larger fiber diameter. According to SEM images of fibers, uniform fibers with controlled morphology and no bead formation (or defects) were obtained. SEM micrographs showed that adding curcumin to PHBV/PCL solution increased fiber diameter from 497 nm to 1200 nm, as shown in Figure 12. The increasing viscosity of the solution, which acts as reinforcement in the PHBV/PCL matrix, explains this.

The morphology and frequency of fiber distribution did not change significantly when the curcumin concentration was increased to 5% w/w. Curcumin aggregates were not present on the surface of the fibers. Previous research using human skin fibroblast cells showed that fibroblast proliferation and gene expression are influenced by fiber diameter. The most effective fibers for fibroblast proliferation and matrix deposition were found to be those with diameters of 350–1100 nm [102]. This supports our hypothesis that curcumin-loaded fibrous scaffolds may be beneficial in wound healing.

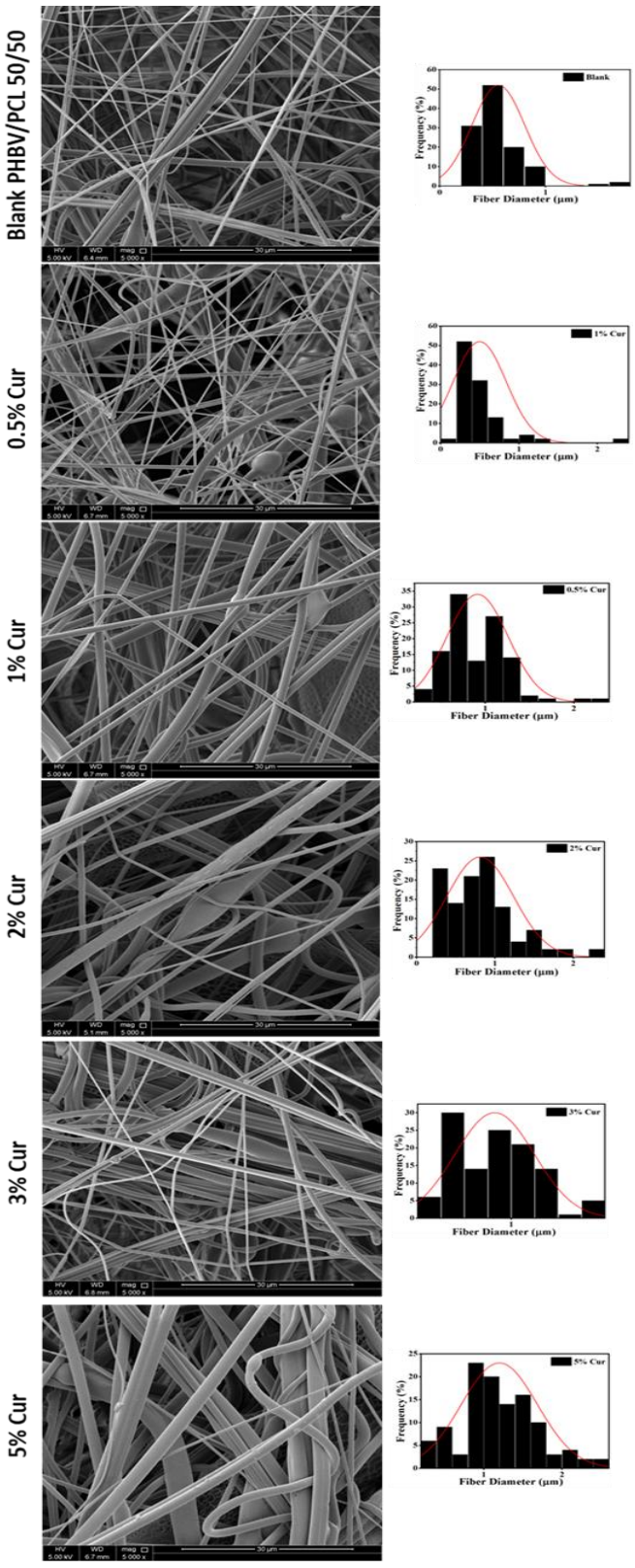

Figure 12. SEM images of blank and curcumin-loaded nanofibers (0.5%, 1%, 2%, 3% and 5% Curcumin). Fiber diameter distributions of curcumin-loaded fibers are visualized at the edges of the SEM images (n=100).

Table 4. Statistical tabulation of Fiber diameters of the curcumin-loaded membranes (n=100)

Composition	Mean (µm)	S.D (µm)	Minimum (µm)	Median (µm)	Maximum (µm)
Blank PHBV/PCL	0.497	0.338	0.192	0.405	2.338
0.5% Cur	0.529	0.414	0.127	0.474	2.753
1% Cur	0.911	0.346	0.277	0.827	2.298
2% Cur	0.811	0.426	0.22	0.7855	2.222
3% Cur	0.858	0.339	0.327	0.832	1.766
5% Cur	1.199	0.485	0.306	1.0935	2.442

XRD

Curcumin and PHBV/PCL X-ray diffraction patterns, as well as Curcumin-loaded fibers, are shown in Figure 13. Pure curcumin is a crystalline substance with a range of distinct reflections ranging from 10◦ to 30◦ 2θ. As discussed in the previous analysis of PHBV/PCL blend optimization, blank PHBV/PCL shows only two prominent peaks, which are indicative of the crystalline nature of PCL presence in the blend. Tiny diffraction peaks in the Curcumin-loaded PHBV/PCL XRD patterns can be due to raw curcumin, indicating that some curcumin is still present in a crystalline state in the fibers. The characteristic two peaks of curcumin between 10◦ to 30◦ 2θ begin to appear in the samples at higher concentrations of Curcumin (above 2%). The 5 % Curcumin shows these peaks very clearly. The increased presence of crystalline curcumin nanoparticles in the samples can be due to this.

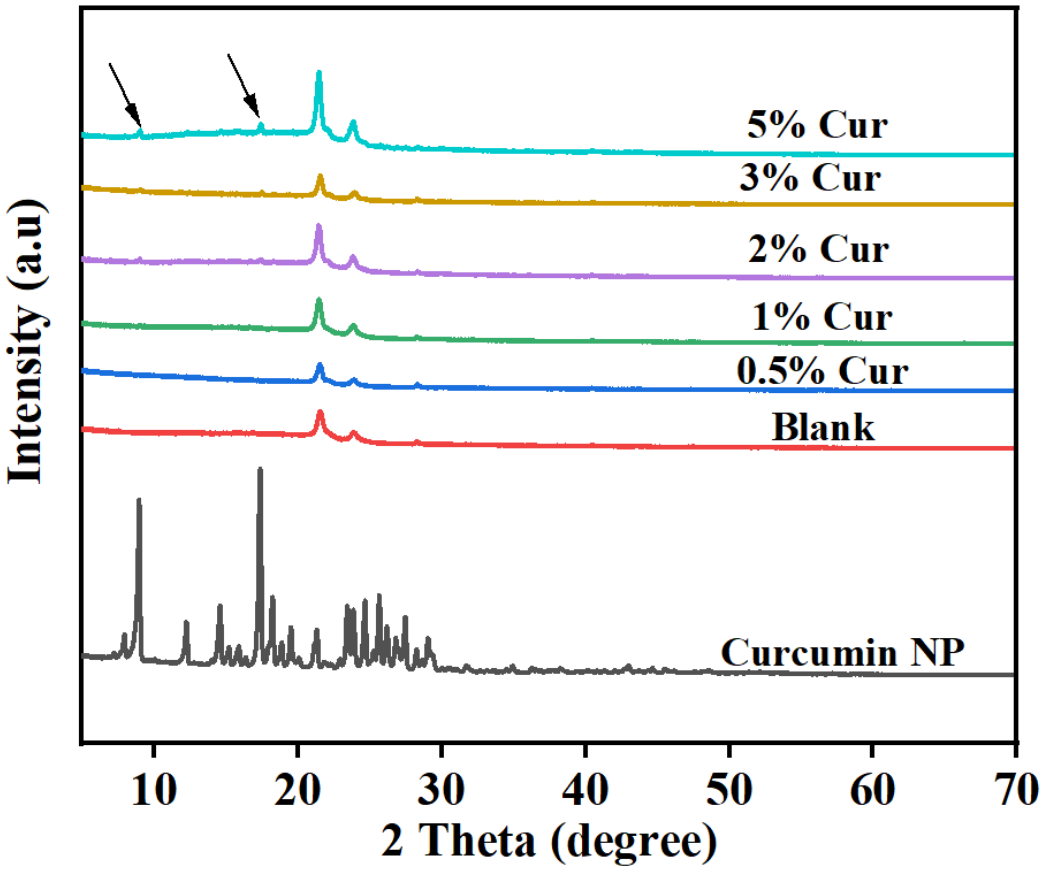

Figure 13. XRD spectra of curcumin nanoparticles, blank PHBV/PCL sample and curcumin-loaded samples to check the crystalline/amorphous nature of the incorporated curcumin into the matrix

DSC

Table 5 summarizes the thermal transition temperatures of the blank and curcumin-loaded samples. Thermograms of PHBV/PCL and curcumin-loaded PHBV/PCL are shown in Figure 14. The thermogram of curcumin-loaded PHBV/PCL fibers shows a large endothermic peak between 50 and 60 ^{o}C due to water loss, as well as two endothermic peaks between 165 and 180 ^{o}C, which correspond to the melting temperatures (Tm) of curcumin and PHBV/PCL, respectively. In accordance with the findings of X-ray diffraction, a phase distinction between the two components in the fiber is clearly visible here. The Tm peak of curcumin at 175 ^{o}C is not visible in the

thermogram of the PHBV/PCL fibers, indicating the generation of a homogeneous system. With rising curcumin concentration, the water evaporation endotherm has also moved to a higher temperature, from 90 to 100 ^{o}C. This is due to molecules in PHBV/PCL taking over some of the water molecules' binding sites. The findings can be explained in terms of the fibers' local structure. The curcumin was at least partly present in a crystalline state in the fibers, according to both XRD and DSC. The amount of crystallinity of PHBV and PCL polymers present in the fibers decreases as the drug content increases.

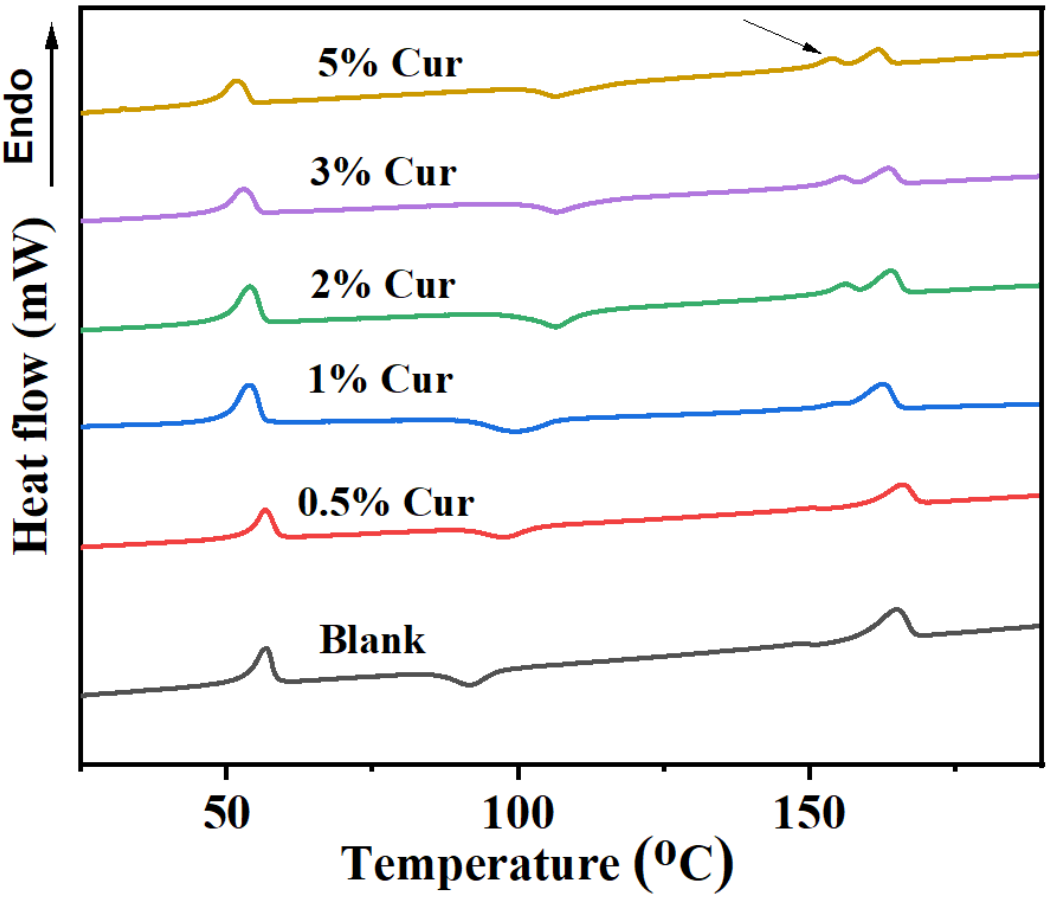

Figure 14. DSC heating thermograms of blank PHBV/PCL and curcumin-loaded samples to analyze the thermal behavior and influence on crystallinity

Table 5. DSC parameters for curcumin-loaded PHBV/PCL membranes. T_c is crystallization temperature from cooling pass, T_m is melting temperature from the heating pass and X is the crystallinity % of the specific polymer

Sample	PHBV			PCL		
	Tc(°C)	Tm (°C)	X (%)	Tc(°C)	Tm (°C)	X (%)
Blank PHBV/PCL	0	164.9	43.98	30.8	56.7	24.56
0.5% Curcumin	0	166.0	31.58	30.3	56.4	26.22
1% Curcumin	0	162.7	32.35	24.2	53.8	29.12
2% Curcumin	0	164.0	30.84	22.4	53.8	28.13
3% Curcumin	0	163.5	28.33	21.5	52.9	24.19
5% Curcumin	0	161.8	27.25	20.9	51.6	26.90

FTIR

The FT-IR spectra of blank PHBV/PCL, curcumin, and curcumin-loaded PHBV/PCL fibers are shown in Figure 15. According to the results obtained for PHBV/PCL composite scaffolds mentioned in the previous study, chemical functional groups for the samples were very close. The absorption of the saturated ester groups appeared as follows in the curcumin spectra (**Figure 15**): 806 cm^{-1}, 873 cm^{-1}, 955 cm^{-1}, 1113 cm^{-1}, 1164 cm^{-1}, 1214 cm^{-1}, 1214 cm^{-1}, 1214 cm^{-1}, 1214 cm^{-1}, 1214 cm^{-1}, 1214 cm^{-1}, 1214 cm^{-1}, 1214 cm^{-1}, 1214 cm^{-1}, 1214 cm^{-1}. The hydroxyl group's stretching area appeared in the band range of 3200-3550 cm^{-1}. Curcumin's band of alkanes (C-H). Curcumin's wavenumber was found to be 1501 cm^{-1}. The existence of an ether group was

suggested by stretching bands at 1000-1260 cm^{-1} (C-O). Curcumin's vibration of the C-O stretching band was distinguished by a spectrum at about 1162 cm^{-1}. Curcumin's characteristic peak at 3500 cm^{-1} was absent from the spectrum of curcumin-loaded PHBV/PCL nanofiber [103].

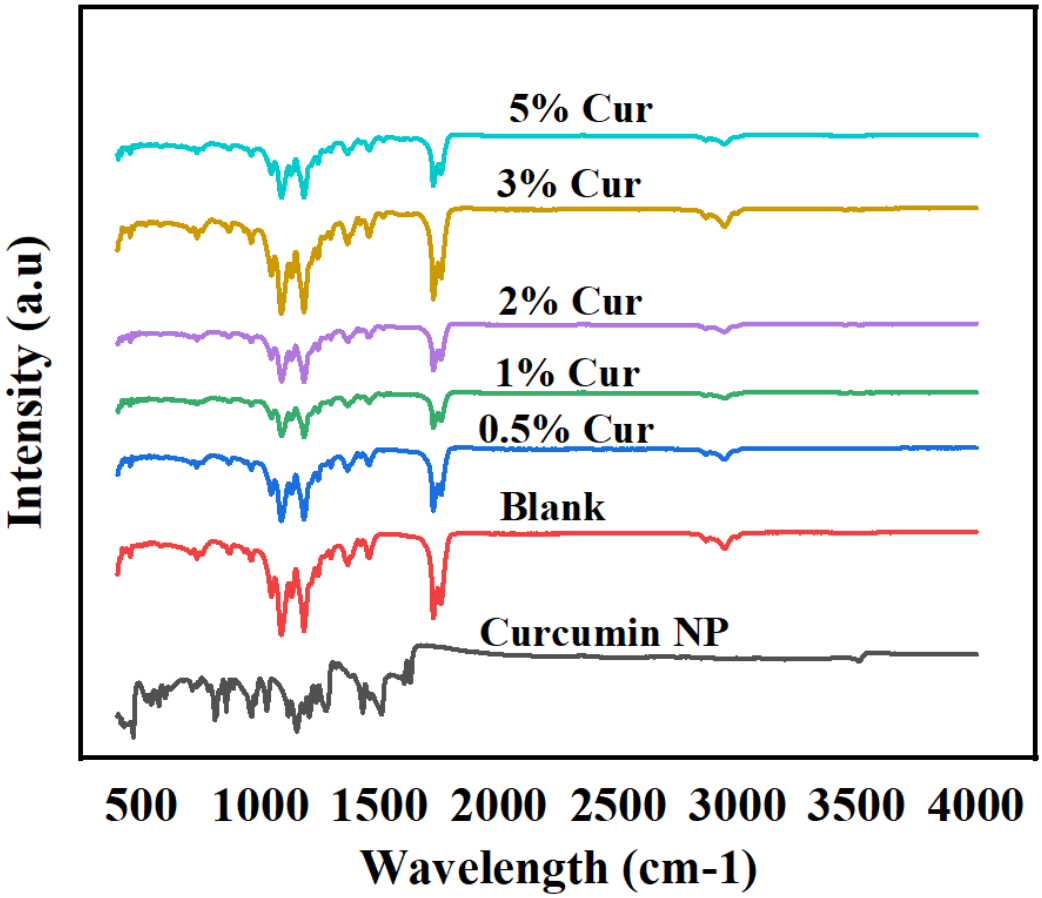

Figure 15. FTIR spectra of blank and curcumin-loaded PHBV/PCL samples to assess new chemical bond formations

Water retention study

Swelling experiments are preliminary tests for determining if biodegradable polymers are compatible. The fibrous scaffolds' ability to absorb vast amounts of water and swell as a result makes them a good choice for use in living tissues, giving them

unique physical properties. The water uptake of samples was investigated using the swelling capability of prepared fibers. In numerous studies, highly swelling matrices have been shown to benefit cell attachment, growth, and internal migration into three-dimensional scaffolds. The addition of curcumin significantly improved the swelling ratio, according to research. With increasing curcumin concentration, the swelling ratio of curcumin-loaded PHBV/PCL fibers clearly increased from around 10 to around 17. The swelling ratio of PHBV/PCL containing 3% curcumin was the largest, at 17. This might be due to the combination of best hydrophobicity and porosity which gave the high value of swelling ratio. Furthermore, this finding may help improve cell attachment and proliferation on PHBV/PCL fibers (**Figure 16**).

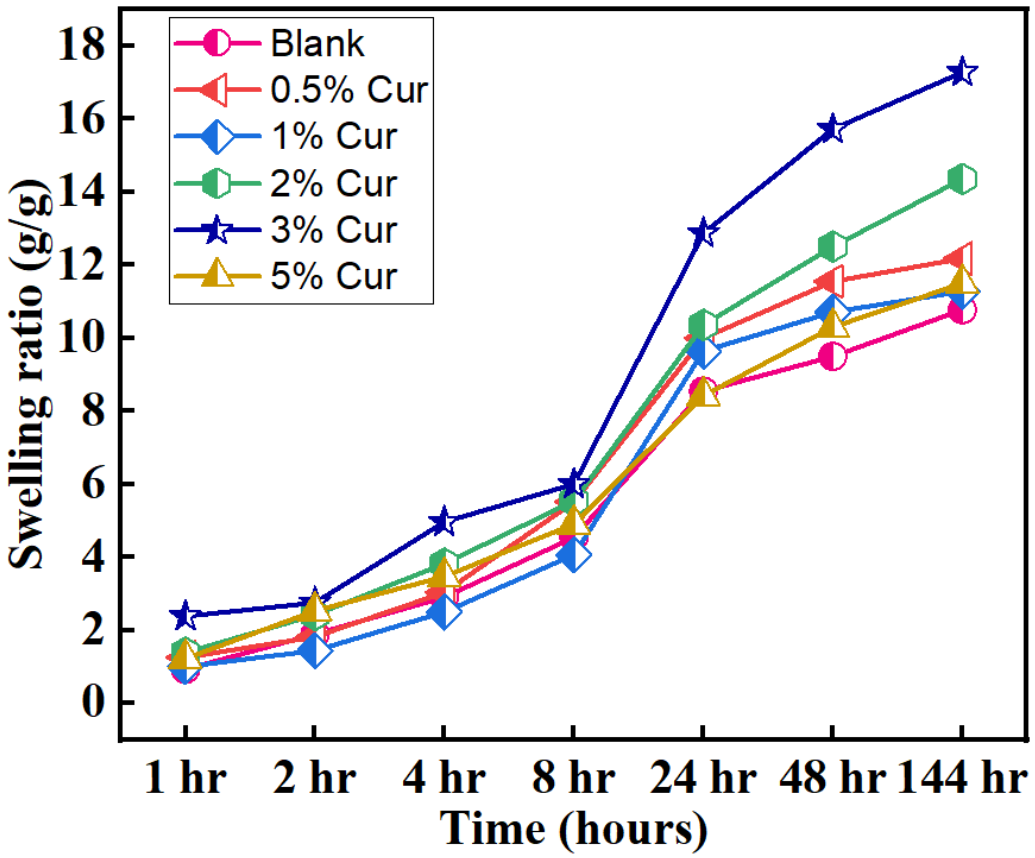

Figure 16. Water retention capacity of blank and curcumin-loaded samples of PHBV/PCL in terms of swelling ratio

4.2.2 *In Vitro* cell studies

MTT assay

The colorimetric MTT assay detects viable cells converting MTT tetrazolium molecules to a purple formazan product, which indicates normal mitochondrial activity. As a result, the rate at which MTT is converted into the purple formazan component by living cells can be used to estimate cellular metabolism. After 24 hours of cell culture, the optical density of each sample was determined and displayed. Curcumin-loaded PHBV/PCL fibers were found to have strong biocompatibility and to promote cell growth and proliferation. The following was the order of cell viability at the end of the 24-hour extraction: 5% Cur < 3% Cur < 2% Cur < 1% Cur < Blank

PHBV/PCL < Cur 0.5%. With a concentration of 0.5 % curcumin, there is a favorable trend in cell viability (**Figure 17**). The viability of the cells in the 0.5 % curcumin-loaded fiber wells was clearly higher than that of the plain PHBV/PCL fibers, and the cells proliferated 8% more than the control. Curcumin's effect on cell signaling pathways of cell attachment resulted in an increase in cell proliferation. The effects of curcumin concentration on cell viability have been recorded in a wide range of ways. Curcumin has a beneficial impact on cell attachment when it is less than 25 mmol/L, according to Merrell et al.[104]. Curcumin plays an important role in enhancing cell attachment and proliferation by increasing cell signaling pathways in neighboring cells. It's worth noting that, as reported in a few previous studies, the lower cell growth on fibers compared to blank is most likely due to slow cell proliferation on foreign materials, even biocompatible ones. The viability of 3T3 fibroblasts decreased as the content was increased beyond 0.5 %. This preliminary analysis of the curcumin-loaded PHBV/PCL fibers indicates that scaffolds with curcumin concentrations greater than 0.5 % in the fibrous scaffolds are toxic to the cells. This is in conformity with the previous discussions where it was shown that the curcumin was present in the matrix as distinct crystalline entity. The crystalline curcumin was more evident in higher concentrations of curcumin samples which might have resulted in the easy release of curcumin from the samples. This quick degradation release in large amounts must have been toxic to the cell viability.

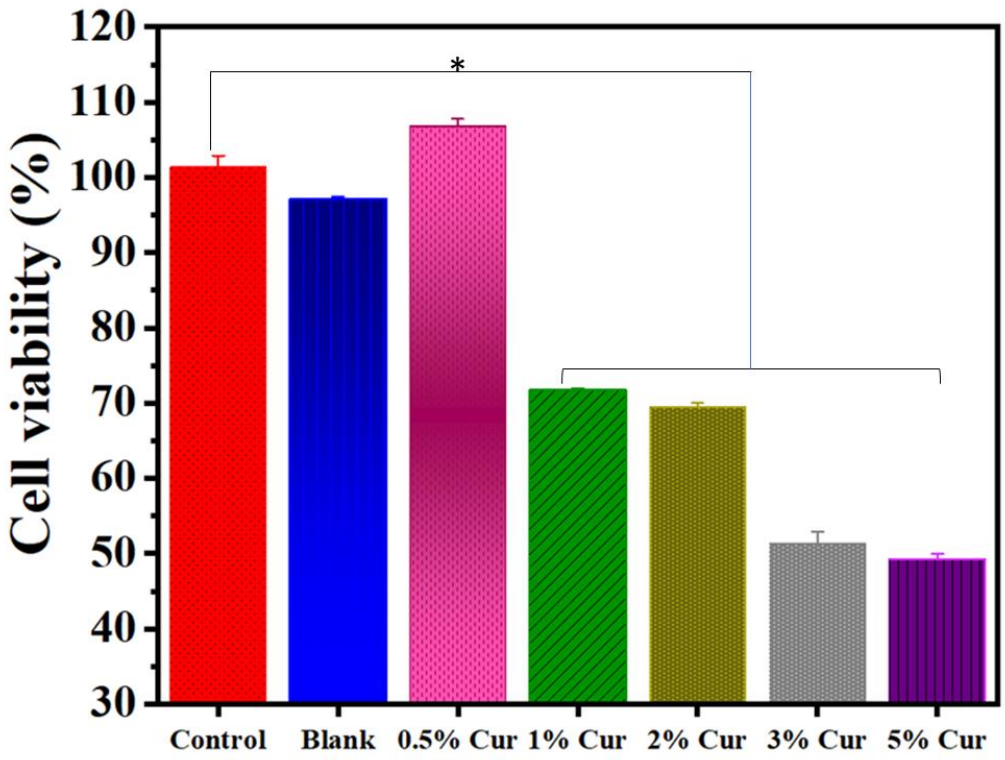

Figure 17 Viability of 3T3 fibroblast cells cultured on blank PHBV/PCL and curcumin-loaded PHBV/PCL fibre mats after 24 h. Viability was significantly reduced by curcumin, although > 50% of cells remained viable on all scaffolds. Data are the mean ± SD. (* $p<0.05$)

Scratch assay

In vitro, the wound healing scratch test may be used to see whether wound dressing materials help or hinder wound healing. The effect of curcumin on cell migration was investigated using a scratch assay and the ability of the cells to migrate in the presence of a nanofibrous mat (**Figure 18**). Cells were seeded at 8 x 10^5 cells per well and starved in imperfect media at first.

Figure 19 depicts the scratch assay findings in terms of wound contraction area obtained via the scratch procedure. Since 3T3 cells migrated into the scratched area

after 24 hours of scaffold therapy, about 30% of the scratched area healed in charge. On the PHBV/PCL membranes, a relatively similar pattern of about 25% wound contraction was observed. As compared to pure PHBV/PCL scaffolds and control groups, Curcumin-loaded scaffold groups containing less than 1% curcumin significantly improved scratch healing. Scaffolds containing more than 1% curcumin decreased the %age of wound contraction. This is due to the toxicity of increased curcumin supply, as stated in the previous MTT report. In the in vitro wound model, it was discovered that 0.5 % curcumin containing PHBV/PCL scaffolds increased cell migration the most. This behavior can be attributed to the same factors as discussed in the preceding section.

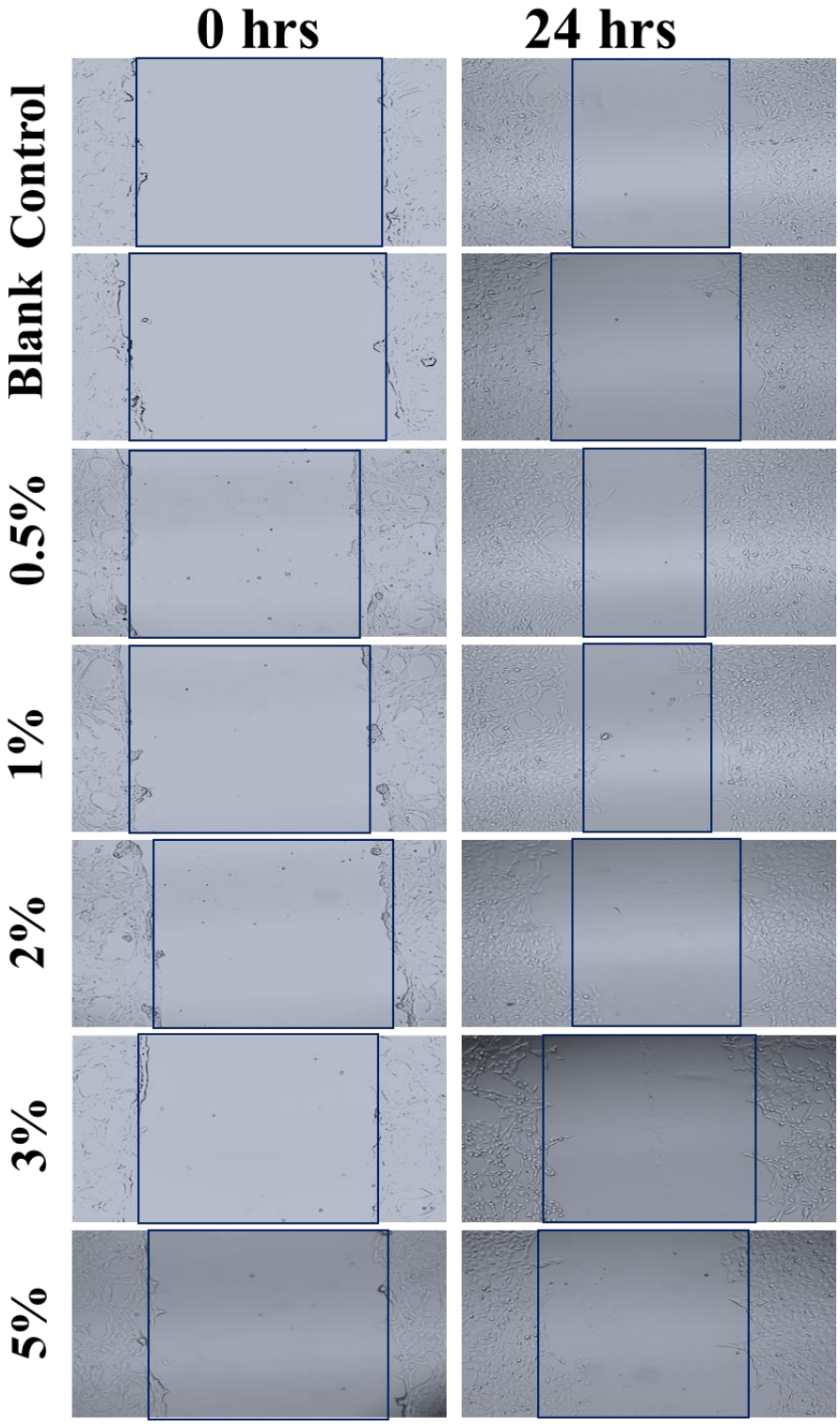

Figure 18. Cell migration and wound contraction results of developed patches in vitro for 3T3 fibroblast. The images of in vitro wound healing were taken using 4× magnification. Navy blue boxes indicate the boundary of the wounds before sample treatment and after 24 h of treatment.

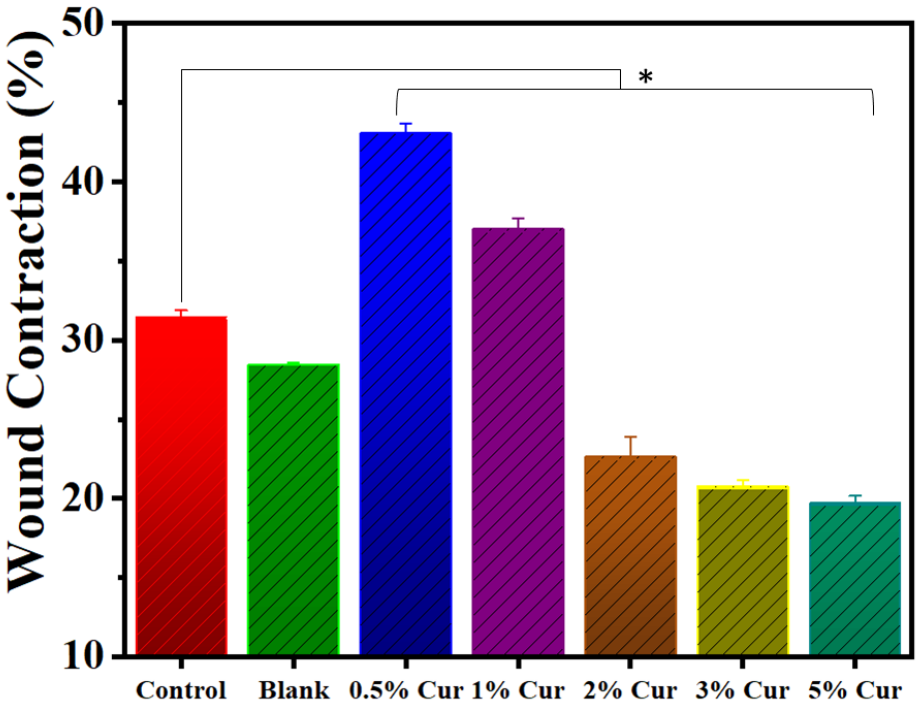

Figure 19. Percentage wound closure of scratch wounds after 24 hours. The wound closure rate was significantly higher for 0.5% and 1%(w/w) curcumin dressings after 24 hours compared with control. Data are the mean±SD.

4.2.3 Inferences

Various concentrations of curcumin were incorporated into air-jet spun PHBV/PCL fibers. The fibers showed continuous morphology with increasing trend of fiber diameter with increasing curcumin content. The XRD, FTIR, DSC results showed that the curcumin nanoparticles were properly incorporated into the matrix and exhibited crystalline form. The water retention study showed that the curcumin incorporation increases the water uptake capacity for all the samples. In comparison to the control group, the results of the cytotoxicity and migration assay analysis show that CURCUMIN impregnated PHBV/PCL membranes provide a robust environment that promotes wound healing in an in vitro model. The proliferation and migration of fibroblast (3T3) cells were significantly increased, which may be one of the reasons

for the re-epithelialization process to be accelerated. In the in vitro wound model, it was discovered that 0.5 % curcumin containing PHBV/PCL scaffolds increased cell migration the most.

More in-depth studies need to be carried out to better assess the toxicity of curcumin in wound healing application. More *in vitro* and *in vivo* studies will help us make more robust conclusions on the viability of using curcumin as active agents in wound healing materials. Otherwise, the above results showing the toxic nature of higher %age of curcumin in the biomaterials can be directed towards their use in anti-cancer studies.

Chapter 5: Conclusions

In the first chapter, detailed literature review of various fabrication techniques being used for fabrication of biomaterials for wound healing applications were discussed. Air-jet spinning was introduced as a better alternative to electrospinning to fabricate fibrous biomaterials for wound healing applications. Following this, PCL, PHBV and the blend of PHBV/PCL membranes for wound healing applications were explored. Furthermore, the role of Curcumin was thoroughly described in terms of wound healing. The materials and methods for fabrication of PHBV/PCL and loading of curcumin into the PHBV/PCL matrix was described. The various physio-chemical characterization studies were described to assess the quality of the fibers. Various cell culture studies that would help to determine the suitability of the fabricate materials in wound healing applications were also discussed. From the first study, it was concluded that increasing the PHBV concentration increases the cell viability and proliferation properties of the air-jet spun samples, and the PCL concentration imparts mechanical strength properties to the air-jet spun samples. From the water retention study, tensile strength study and cell adhesion study, it can be reasonably concluded that PHBV/PCL 50/50 shows the best combination of mechanical and biologically favoring properties among all the compositions studied of PHBV/PCL. In the next study, various concentrations of curcumin were incorporated into air-jet spun PHBV/PCL fibers. The fibers showed continuous morphology with increasing trend of fiber diameter with increasing curcumin content. The XRD, FTIR, DSC results showed that the curcumin nanoparticles were properly incorporated into the matrix and exhibited crystalline form. The water retention study showed that the curcumin incorporation increases the water uptake capacity for all the samples. The results

obtained from cytotoxicity and migration assay study shows that CURCUMIN impregnated PHBV/PCL membranes provide a robust environment that promotes wound healing in an *In vitro* model as compared to control group. The proliferation and migration of fibroblast (3T3) cells was significantly increased that may be one of the triggers to boost the re-epithelialization process. Overall, it has been observed that 0.5% curcumin containing PHBV/PCL scaffolds improved the cell migration the most for the in vitro wound model.

Having low mechanical strength (significantly less than electrospun membranes), especially for natural polymer-based membranes, prevents the widespread use of the otherwise beneficial functions of air-jet spun nanofibers. Incorporation of various nanofillers in polymer matrix and blending with mechanically robust polymers are tried as the potential strategies to improve the mechanical properties of spun membranes. However, exactly mimicking the mechanical properties of spun membranes with that of ECM of various tissues is still challenging. Future research may focus on this direction where tissue specific ECM mimetic scaffolds with matching tensile strength, modulus and elasticity will be developed.

References

[1] Y. Huang and T. R. Kyriakides, “The role of extracellular matrix in the pathophysiology of diabetic wounds,” *Matrix Biol. Plus*, 2020, doi: 10.1016/j.mbplus.2020.100037.

[2] E. Lorenzo-Martín, P. Gallego-Muñoz, S. Mar, I. Fernández, P. Cidad, and M. C. Martínez-García, “Dynamic changes of the extracellular matrix during corneal wound healing,” *Exp. Eye Res.*, vol. 186, Sep. 2019, doi: 10.1016/j.exer.2019.107704.

[3] A. Figueiredo, E. C. Leal, and E. Carvalho, “Protein tyrosine phosphatase 1B inhibition as a potential therapeutic target for chronic wounds in diabetes,” *Pharmacological Research*, vol. 159. Academic Press, Sep. 01, 2020, doi: 10.1016/j.phrs.2020.104977.

[4] P. K. Prabhakar, K. Singh, D. Kabra, and J. Gupta, “Natural SIRT1 modifiers as promising therapeutic agents for improving diabetic wound healing,” *Phytomedicine*, vol. 76. Elsevier GmbH, Sep. 01, 2020, doi: 10.1016/j.phymed.2020.153252.

[5] A. D. Theocharis, S. S. Skandalis, C. Gialeli, and N. K. Karamanos, “Extracellular matrix structure,” *Adv. Drug Deliv. Rev.*, vol. 97, pp. 4–27, 2016, doi: 10.1016/j.addr.2015.11.001.

[6] N. U. B. Hansen, F. Genovese, D. J. Leeming, and M. A. Karsdal, “The importance of extracellular matrix for cell function and in vivo likeness,” *Exp. Mol. Pathol.*, vol. 98, no. 2, pp. 286–294, 2015, doi: 10.1016/j.yexmp.2015.01.006.

[7] M. P. Nikolova and M. S. Chavali, “Recent advances in biomaterials for 3D scaffolds: A review,” *Bioact. Mater.*, vol. 4, no. October, pp. 271–292, 2019,

doi: 10.1016/j.bioactmat.2019.10.005.

[8] R. Augustine, E. A. Dominic, I. Reju, B. Kaimal, N. Kalarikkal, and S. Thomas, "Electrospun polycaprolactone membranes incorporated with ZnO nanoparticles as skin substitutes with enhanced fibroblast proliferation and wound healing," *RSC Adv.*, vol. 4, no. 47, pp. 24777–24785, Jun. 2014, doi: 10.1039/c4ra02450h.

[9] R. Augustine, E. A. Dominic, I. Reju, B. Kaimal, N. Kalarikkal, and S. Thomas, "Electrospun poly(ε-caprolactone)-based skin substitutes: *I n vivo* evaluation of wound healing and the mechanism of cell proliferation," *J. Biomed. Mater. Res. Part B Appl. Biomater.*, vol. 103, no. 7, pp. 1445–1454, Oct. 2015, doi: 10.1002/jbm.b.33325.

[10] R. Augustine *et al.*, "Electrospun polyvinyl alcohol membranes incorporated with green synthesized silver nanoparticles for wound dressing applications," *J. Mater. Sci. Mater. Med.*, vol. 29, no. 11, pp. 1–16, Nov. 2018, doi: 10.1007/s10856-018-6169-7.

[11] R. Augustine *et al.*, "Growth factor loaded in situ photocrosslinkable poly(3-hydroxybutyrate-co-3-hydroxyvalerate)/gelatin methacryloyl hybrid patch for diabetic wound healing," *Mater. Sci. Eng. C*, vol. 118, p. 111519, Jan. 2021, doi: 10.1016/j.msec.2020.111519.

[12] M. Liu, X. P. Duan, Y. M. Li, D. P. Yang, and Y. Z. Long, "Electrospun nanofibers for wound healing," *Mater. Sci. Eng. C*, vol. 76, pp. 1413–1423, 2017, doi: 10.1016/j.msec.2017.03.034.

[13] M. Z. Elsabee, H. F. Naguib, and R. E. Morsi, "Chitosan based nanofibers, review," *Materials Science and Engineering C*. 2012, doi: 10.1016/j.msec.2012.05.009.

[14] K. Ye, H. Kuang, Z. You, Y. Morsi, and X. Mo, "Electrospun nanofibers for

tissue engineering with drug loading and release," *Pharmaceutics*, 2019, doi: 10.3390/pharmaceutics11040182.

[15] M. Mabrouk, H. H. Beherei, and D. B. Das, "Recent progress in the fabrication techniques of 3D scaffolds for tissue engineering," *Mater. Sci. Eng. C*, vol. 110, p. 110716, 2020, doi: 10.1016/j.msec.2020.110716.

[16] P. Yin, H. M. T. Choi, C. R. Calvert, and N. A. Pierce, "Programming biomolecular self-assembly pathways," *Nature*, 2008, doi: 10.1038/nature06451.

[17] J. D. Hartgerink, E. Beniash, and S. I. Stupp, "Self-assembly and mineralization of peptide-amphiphile nanofibers," *Science (80-.).*, 2001, doi: 10.1126/science.1063187.

[18] J. D. Hartgerink, E. Beniash, and S. I. Stupp, "Peptide-amphiphile nanofibers: A versatile scaffold for the preparation of self-assembling materials," *Proc. Natl. Acad. Sci. U. S. A.*, 2002, doi: 10.1073/pnas.072699999.

[19] J. B. Matson and S. I. Stupp, "Self-assembling peptide scaffolds for regenerative medicine," *Chem. Commun.*, 2012, doi: 10.1039/c1cc15551b.

[20] Z. Luo, S. Wang, and S. Zhang, "Fabrication of self-assembling d-form peptide nanofiber scaffold d-EAK16 for rapid hemostasis," *Biomaterials*, 2011, doi: 10.1016/j.biomaterials.2010.11.049.

[21] W. Zhang, X. Yu, Y. Li, Z. Su, K. D. Jandt, and G. Wei, "Protein-mimetic peptide nanofibers: Motif design, self-assembly synthesis, and sequence-specific biomedical applications," *Progress in Polymer Science*. 2018, doi: 10.1016/j.progpolymsci.2017.12.001.

[22] X. Liu *et al.*, "Functionalized self-assembling peptide nanofiber hydrogels mimic stem cell niche to control human adipose stem cell behavior in vitro," *Acta Biomater.*, 2013, doi: 10.1016/j.actbio.2013.01.027.

[23] T. Lu, Y. Li, and T. Chen, “Techniques for fabrication and construction of three-dimensional scaffolds for tissue engineering,” *International Journal of Nanomedicine*. 2013, doi: 10.2147/IJN.S38635.

[24] C. P. Barnes, S. A. Sell, E. D. Boland, D. G. Simpson, and G. L. Bowlin, “Nanofiber technology: Designing the next generation of tissue engineering scaffolds,” *Advanced Drug Delivery Reviews*. 2007, doi: 10.1016/j.addr.2007.04.022.

[25] R. M. Allaf, “Melt-molding technologies for 3D scaffold engineering,” in *Functional 3D Tissue Engineering Scaffolds: Materials, Technologies, and Applications*, 2018.

[26] C. Colosi, M. Costantini, A. Barbetta, R. Pecci, R. Bedini, and M. Dentini, “Morphological comparison of PVA scaffolds obtained by gas foaming and microfluidic foaming techniques,” *Langmuir*, 2013, doi: 10.1021/la303788z.

[27] X. Jing, H. Y. Mi, and L. S. Turng, “Comparison between PCL/hydroxyapatite (HA) and PCL/halloysite nanotube (HNT) composite scaffolds prepared by co-extrusion and gas foaming,” *Mater. Sci. Eng. C*, 2017, doi: 10.1016/j.msec.2016.11.049.

[28] P. Liu *et al.*, “3D bioprinting and in vitro study of bilayered membranous construct with human cells-laden alginate/gelatin composite hydrogels,” *Colloids Surfaces B Biointerfaces*, vol. 181, pp. 1026–1034, Sep. 2019, doi: 10.1016/j.colsurfb.2019.06.069.

[29] A. Bagheri and J. Jin, “Photopolymerization in 3D Printing,” *ACS Appl. Polym. Mater.*, 2019, doi: 10.1021/acsapm.8b00165.

[30] J. A. Inzana *et al.*, “3D printing of composite calcium phosphate and collagen scaffolds for bone regeneration,” *Biomaterials*, 2014, doi:

10.1016/j.biomaterials.2014.01.064.

[31] K. K. Moncal, V. Ozbolat, P. Datta, D. N. Heo, and I. T. Ozbolat, “Thermally-controlled extrusion-based bioprinting of collagen,” *J. Mater. Sci. Mater. Med.*, 2019, doi: 10.1007/s10856-019-6258-2.

[32] H. K. Kleinman, L. Luckenbill-Edds, F. W. Cannon, and G. C. Sephel, “Use of extracellular matrix components for cell culture,” *Analytical Biochemistry*. 1987, doi: 10.1016/0003-2697(87)90538-0.

[33] F. Blaudez, S. Ivanovski, S. Hamlet, and C. Vaquette, “An overview of decellularisation techniques of native tissues and tissue engineered products for bone, ligament and tendon regeneration,” *Methods*, vol. 171, no. August, pp. 28–40, 2020, doi: 10.1016/j.ymeth.2019.08.002.

[34] H. H. Elmashhady, B. A. Kraemer, K. H. Patel, S. A. Sell, and K. Garg, “Decellularized extracellular matrices for tissue engineering applications,” *Electrospinning*, 2017, doi: 10.1515/esp-2017-0005.

[35] L. K. Y. Chan, V. Y. L. Leung, V. Tam, W. W. Lu, K. Y. Sze, and K. M. C. Cheung, “Decellularized bovine intervertebral disc as a natural scaffold for xenogenic cell studies,” *Acta Biomater.*, 2013, doi: 10.1016/j.actbio.2012.09.005.

[36] K. P. Feltz, E. A. G. Kalaf, C. Chen, R. S. Martin, and S. A. Sell, “A review of electrospinning manipulation techniques to direct fiber deposition and maximize pore size,” *Electrospinning*, 2017, doi: 10.1515/esp-2017-0002.

[37] A. D. Juncos Bombin, N. J. Dunne, and H. O. McCarthy, “Electrospinning of natural polymers for the production of nanofibres for wound healing applications,” *Materials Science and Engineering C*, vol. 114. Elsevier Ltd, Sep. 01, 2020, doi: 10.1016/j.msec.2020.110994.

[38] W. E. Teo, W. He, and S. Ramakrishna, “Electrospun scaffold tailored for tissue-specific extracellular matrix,” *Biotechnology Journal*. 2006, doi: 10.1002/biot.200600044.

[39] Y. Z. Zhang, B. Su, J. Venugopal, S. Ramakrishna, and C. T. Lim, “Biomimetic and bioactive nanofibrous scaffolds from electrospun composite nanofibers,” *International Journal of Nanomedicine*. 2007.

[40] D. Grande, J. Ramier, D. L. Versace, E. Renard, and V. Langlois, “Design of functionalized biodegradable PHA-based electrospun scaffolds meant for tissue engineering applications,” *N. Biotechnol.*, 2017, doi: 10.1016/j.nbt.2016.05.006.

[41] C. Burger and B. Chu, “Functional nanofibrous scaffolds for bone reconstruction,” *Colloids Surfaces B Biointerfaces*, 2007, doi: 10.1016/j.colsurfb.2006.09.023.

[42] R. Nayak, R. Padhye, I. L. Kyratzis, Y. B. Truong, and L. Arnold, “Recent advances in nanofibre fabrication techniques,” *Text. Res. J.*, 2012, doi: 10.1177/0040517511424524.

[43] X. Liu *et al.*, “In vivo wound healing and antibacterial performances of electrospun nanofibre membranes,” *J. Biomed. Mater. Res. - Part A*, 2010, doi: 10.1002/jbm.a.32718.

[44] B. Bagheri *et al.*, “Tissue engineering with electrospun electro-responsive chitosan-aniline oligomer/polyvinyl alcohol,” *Int. J. Biol. Macromol.*, vol. 147, pp. 160–169, 2020, doi: 10.1016/j.ijbiomac.2019.12.264.

[45] C. J. Luo, S. D. Stoyanov, E. Stride, E. Pelan, and M. Edirisinghe, “Electrospinning versus fibre production methods: From specifics to technological convergence,” *Chem. Soc. Rev.*, 2012, doi: 10.1039/c2cs35083a.

[46] K. M. Woo, V. J. Chen, and P. X. Ma, “Nano-fibrous scaffolding architecture

selectively enhances protein adsorption contributing to cell attachment," *J. Biomed. Mater. Res. - Part A*, vol. 67, no. 2, pp. 531–537, Nov. 2003, doi: 10.1002/jbm.a.10098.

[47] W. E. Teo, R. Inai, and S. Ramakrishna, "Technological advances in electrospinning of nanofibers," *Science and Technology of Advanced Materials*. 2011, doi: 10.1088/1468-6996/12/1/013002.

[48] A. Khalf and S. V. Madihally, "Recent advances in multiaxial electrospinning for drug delivery," *European Journal of Pharmaceutics and Biopharmaceutics*. 2017, doi: 10.1016/j.ejpb.2016.11.010.

[49] S. Thakkar and M. Misra, "Electrospun polymeric nanofibers: New horizons in drug delivery," *European Journal of Pharmaceutical Sciences*. 2017, doi: 10.1016/j.ejps.2017.07.001.

[50] N. Zhang *et al.*, "Biomimicking Fiber Scaffold as an Effective In Vitro and In Vivo MicroRNA Screening Platform for Directing Tissue Regeneration," *Adv. Sci.*, vol. 6, no. 9, 2019, doi: 10.1002/advs.201800808.

[51] L. H. Nguyen, M. Gao, J. Lin, W. Wu, J. Wang, and S. Y. Chew, "Three-dimensional aligned nanofibers-hydrogel scaffold for controlled non-viral drug/gene delivery to direct axon regeneration in spinal cord injury treatment," *Sci. Rep.*, vol. 7, p. 42212, 2017, doi: 10.1038/srep42212.

[52] M. Zamani, M. P. Prabhakaran, and S. Ramakrishna, "Advances in drug delivery via electrospun and electrosprayed nanomaterials," *International Journal of Nanomedicine*. 2013, doi: 10.2147/IJN.S43575.

[53] Y. Lu *et al.*, "Coaxial electrospun fibers: applications in drug delivery and tissue engineering," *Wiley Interdisciplinary Reviews: Nanomedicine and Nanobiotechnology*. 2016, doi: 10.1002/wnan.1391.

[54] I. Yalcin Enis and T. Gok Sadikoglu, “Design parameters for electrospun biodegradable vascular grafts,” *Journal of Industrial Textiles*. 2018, doi: 10.1177/1528083716654470.

[55] A. Hasan *et al.*, “Electrospun scaffolds for tissue engineering of vascular grafts,” *Acta Biomaterialia*. 2014, doi: 10.1016/j.actbio.2013.08.022.

[56] J. Hu *et al.*, “Electrospinning of poly(glycerol sebacate)-based nanofibers for nerve tissue engineering,” *Mater. Sci. Eng. C*, 2017, doi: 10.1016/j.msec.2016.03.035.

[57] J. I. Kim, T. I. Hwang, L. E. Aguilar, C. H. Park, and C. S. Kim, “A Controlled Design of Aligned and Random Nanofibers for 3D Bi-functionalized Nerve Conduits Fabricated via a Novel Electrospinning Set-up,” *Sci. Rep.*, 2016, doi: 10.1038/srep23761.

[58] U. Milbreta *et al.*, “Three-Dimensional Nanofiber Hybrid Scaffold Directs and Enhances Axonal Regeneration after Spinal Cord Injury,” *ACS Biomater. Sci. Eng.*, vol. 2, no. 8, pp. 1319–1329, 2016, doi: 10.1021/acsbiomaterials.6b00248.

[59] U. Stachewicz *et al.*, “3D imaging of cell interactions with electrospun PLGA nanofiber membranes for bone regeneration,” *Acta Biomater.*, 2015, doi: 10.1016/j.actbio.2015.09.003.

[60] D. P. Bhattarai, L. E. Aguilar, C. H. Park, and C. S. Kim, “A review on properties of natural and synthetic based electrospun fibrous materials for bone tissue engineering,” *Membranes*. 2018, doi: 10.3390/membranes8030062.

[61] D. Pankajakshan, M. T. P. Albuquerque, and M. C. Bottino, “Electrospun nanofibers for regenerative dentistry,” in *Electrospun Materials for Tissue Engineering and Biomedical Applications: Research, Design and Commercialization*, 2017.

[62] J. Fernández-Pérez, K. E. Kador, A. P. Lynch, and M. Ahearne, "Characterization of extracellular matrix modified poly(ε-caprolactone) electrospun scaffolds with differing fiber orientations for corneal stroma regeneration," *Mater. Sci. Eng. C*, 2020, doi: 10.1016/j.msec.2019.110415.

[63] Z. Arabpour *et al.*, "Design and characterization of biodegradable multi layered electrospun nanofibers for corneal tissue engineering applications," *J. Biomed. Mater. Res. - Part A*, 2019, doi: 10.1002/jbm.a.36742.

[64] J. B. Rose *et al.*, "In vitro evaluation of electrospun blends of gelatin and PCL for application as a partial thickness corneal graft," *J. Biomed. Mater. Res. - Part A*, 2019, doi: 10.1002/jbm.a.36598.

[65] T. Zhou *et al.*, "Electrospun tilapia collagen nanofibers accelerating wound healing via inducing keratinocytes proliferation and differentiation," *Colloids Surfaces B Biointerfaces*, 2016, doi: 10.1016/j.colsurfb.2016.03.052.

[66] L. J. Gould, "Topical Collagen-Based Biomaterials for Chronic Wounds: Rationale and Clinical Application," *Advances in Wound Care*. 2016, doi: 10.1089/wound.2014.0595.

[67] S. Ahmadian, M. Ghorbani, and F. Mahmoodzadeh, "Silver sulfadiazine-loaded electrospun ethyl cellulose/polylactic acid/collagen nanofibrous mats with antibacterial properties for wound healing," *Int. J. Biol. Macromol.*, vol. 162, pp. 1555–1565, Nov. 2020, doi: 10.1016/j.ijbiomac.2020.08.059.

[68] M. Ghorbani, P. Nezhad-Mokhtari, and S. Ramazani, "Aloe vera-loaded nanofibrous scaffold based on Zein/Polycaprolactone/Collagen for wound healing," *Int. J. Biol. Macromol.*, vol. 153, pp. 921–930, Jun. 2020, doi: 10.1016/j.ijbiomac.2020.03.036.

[69] S. Kandhasamy *et al.*, "Synthesis and Fabrication of Collagen-Coated

Ostholamide Electrospun Nanofiber Scaffold for Wound Healing," *ACS Appl. Mater. Interfaces*, vol. 9, no. 10, pp. 8556–8568, 2017, doi: 10.1021/acsami.6b16488.

[70] L. Sun *et al.*, "Enhanced wound healing in diabetic rats by nanofibrous scaffolds mimicking the basketweave pattern of collagen fibrils in native skin," *Biomater. Sci.*, 2018, doi: 10.1039/c7bm00545h.

[71] K. Yamamoto, G. Murphy, and L. Troeberg, "Extracellular regulation of metalloproteinases," *Matrix Biology*. 2015, doi: 10.1016/j.matbio.2015.02.007.

[72] I. Stamenkovic, "Extracellular matrix remodelling: The role of matrix metalloproteinases," *Journal of Pathology*. 2003, doi: 10.1002/path.1400.

[73] C. Bonnans, J. Chou, and Z. Werb, "Remodelling the extracellular matrix in development and disease," *Nature Reviews Molecular Cell Biology*, vol. 15, no. 12. Nature Publishing Group, pp. 786–801, Dec. 11, 2014, doi: 10.1038/nrm3904.

[74] S. Chen, R. Li, X. Li, and J. Xie, "Electrospinning: An enabling nanotechnology platform for drug delivery and regenerative medicine," *Adv. Drug Deliv. Rev.*, 2018, doi: 10.1016/j.addr.2018.05.001.

[75] R. A. Neal, S. S. Tholpady, P. L. Foley, N. Swami, R. C. Ogle, and E. A. Botchwey, "Alignment and composition of laminin-polycaprolactone nanofiber blends enhance peripheral nerve regeneration," *J. Biomed. Mater. Res. - Part A*, 2012, doi: 10.1002/jbm.a.33204.

[76] R. A. Neal, S. G. McClugage, M. C. Link, L. S. Sefcik, R. C. Ogle, and E. A. Botchwey, "Laminin nanofiber meshes that mimic morphological properties and bioactivity of basement membranes," *Tissue Eng. - Part C Methods*, 2009, doi: 10.1089/ten.tec.2007.0366.

[77] J. Lin *et al.*, “Oriented and sustained protein expression on biomimicking electrospun fibers for evaluating functionality of cells,” *Mater. Sci. Eng. C*, vol. 118, 2021, doi: 10.1016/j.msec.2020.111407.

[78] X. Z. Sun, G. R. Williams, X. X. Hou, and L. M. Zhu, “Electrospun curcumin-loaded fibers with potential biomedical applications,” *Carbohydr. Polym.*, vol. 94, no. 1, pp. 147–153, Apr. 2013, doi: 10.1016/j.carbpol.2012.12.064.

[79] A. M. Abdelgawad, S. M. Hudson, and O. J. Rojas, “Antimicrobial wound dressing nanofiber mats from multicomponent (chitosan/silver-NPs/polyvinyl alcohol) systems,” *Carbohydr. Polym.*, 2014, doi: 10.1016/j.carbpol.2012.12.043.

[80] T. He *et al.*, “Electrospinning polyvinylidene fluoride fibrous membranes containing anti-bacterial drugs used as wound dressing,” *Colloids Surfaces B Biointerfaces*, 2015, doi: 10.1016/j.colsurfb.2015.04.026.

[81] M. Jannesari, J. Varshosaz, M. Morshed, and M. Zamani, “Composite poly(vinyl alcohol)/poly(vinyl acetate) electrospun nanofibrous mats as a novel wound dressing matrix for controlled release of drugs.,” *Int. J. Nanomedicine*, 2011, doi: 10.2147/ijn.s17595.

[82] B. Feng *et al.*, “Bioresorbable electrospun gelatin/polycaprolactone nanofibrous membrane as a barrier to prevent cardiac postoperative adhesion,” *Acta Biomater.*, 2019, doi: 10.1016/j.actbio.2018.10.022.

[83] Z. Wang *et al.*, “Graphene Oxide Incorporated PLGA Nanofibrous Scaffold for Solid Phase Gene Delivery into Mesenchymal Stem Cells,” *J. Nanosci. Nanotechnol.*, 2017, doi: 10.1166/jnn.2018.14362.

[84] A. Abdal-Hay, N. A. M. Barakat, and J. K. Lim, “Novel technique for polymeric nanofibers preparation: Air jet spinning,” *Sci. Adv. Mater.*, vol. 4, no. 12, pp.

1268–1275, 2012, doi: 10.1166/sam.2012.1382.

[85] T. Eren Boncu, A. Uskudar Guclu, M. F. Catma, A. Savaser, A. Gokce, and N. Ozdemir, “In vitro and in vivo evaluation of linezolid loaded electrospun PLGA and PLGA/PCL fiber mats for prophylaxis and treatment of MRSA induced prosthetic infections,” *Int. J. Pharm.*, vol. 573, p. 118758, Jan. 2020, doi: 10.1016/j.ijpharm.2019.118758.

[86] R. Augustine *et al.*, “Titanium Nanorods Loaded PCL Meshes with Enhanced Blood Vessel Formation and Cell Migration for Wound Dressing Applications,” *Macromol. Biosci.*, vol. 24, no. 2, pp. 101–123, 2019, doi: 10.1002/mabi.201900058.

[87] A. Hasan, S. Soliman, F. El Hajj, Y. T. Tseng, H. C. Yalcin, and H. E. Marei, “Fabrication and in Vitro Characterization of a Tissue Engineered PCL-PLLA Heart Valve,” *Sci. Rep.*, 2018, doi: 10.1038/s41598-018-26452-y.

[88] L. Wang, J. Du, D. Cao, and Y. Wang, “Recent Advances and the Application of Poly(3-hydroxybutyrate-co-3-hydroxyvalerate) as Tissue Engineering Materials,” 2013, doi: 10.1080/10601325.2013.802540.

[89] R. Shi *et al.*, “Long-acting and broad-spectrum antimicrobial electrospun poly (ε-caprolactone)/gelatin micro/nanofibers for wound dressing,” *J. Colloid Interface Sci.*, vol. 509, pp. 275–284, Jan. 2018, doi: 10.1016/j.jcis.2017.08.092.

[90] S. Y. H. Abdalkarim, H. Y. Yu, M. L. Song, Y. Zhou, J. Yao, and Q. Q. Ni, “In vitro degradation and possible hydrolytic mechanism of PHBV nanocomposites by incorporating cellulose nanocrystal-ZnO nanohybrids,” *Carbohydr. Polym.*, vol. 176, pp. 38–49, Nov. 2017, doi: 10.1016/j.carbpol.2017.08.051.

[91] D. Daranarong, R. T. H. Chan, N. S. Wanandy, R. Molloy, W. Punyodom, and L. J. R. Foster, “Electrospun polyhydroxybutyrate and poly(L-lactide-co-ε-

caprolactone) composites as nanofibrous scaffolds," *Biomed Res. Int.*, vol. 2014, 2014, doi: 10.1155/2014/741408.

[92] A. T. H Gunes, D Gulen, R Mutlu, A Gumus, T Tas, "Antibacterial effects of curcumin: an in vitro minimum inhibitory concentration study," *Toxicol Ind Heal.*, vol. 32, pp. 246–250, 2016.

[93] K. Z. SZ Moghadamtousi, HA Kadir, P Hassandarvish, H Tajik, S Abubakar, "A review on antibacterial, antiviral, and antifungal activity of curcumin," *Biomed Res Int*, vol. 2014, p. 186864, 2014.

[94] Y. Sun, X. Hu, G. Hu, C. Xu, and H. Jiang, "Curcumin attenuates hydrogen peroxide-induced premature senescence via the activation of SIRT1 in human umbilical vein endothelial cells," *Biol. Pharm. Bull.*, vol. 38, no. 8, pp. 1134–1141, Aug. 2015, doi: 10.1248/bpb.b15-00012.

[95] A. Abdal-Hay, F. A. Sheikh, and J. K. Lim, "Air jet spinning of hydroxyapatite/poly(lactic acid) hybrid nanocomposite membrane mats for bone tissue engineering," *Colloids Surfaces B Biointerfaces*, vol. 102, pp. 635–643, 2013, doi: 10.1016/j.colsurfb.2012.09.017.

[96] A. J. Gallagher, A. N. Anniadh, K. Bruyere, M. Otténio, H. Xie, and M. D. Gilchrist, "Dynamic Tensile Properties of Human Skin."

[97] R. Augustine *et al.*, "Electrospun chitosan membranes containing bioactive and therapeutic agents for enhanced wound healing," *International Journal of Biological Macromolecules*, vol. 156. Elsevier B.V., pp. 153–170, Aug. 01, 2020, doi: 10.1016/j.ijbiomac.2020.03.207.

[98] R. Augustine, S. R. ur Rehman, K. S. Joshy, and A. Hasan, "Stromal cell-derived factor loaded co-electrospun hydrophilic/hydrophobic bicomponent membranes for wound protection and healing," *RSC Adv.*, pp. 572–583, 2021, doi:

10.1039/d0ra04997b.

[99] H. Liu *et al.*, “Blending Modification of PHBV/PCL and its Biodegradation by Pseudomonas mendocina,” *J. Polym. Environ.*, vol. 25, no. 2, pp. 156–164, Jun. 2017, doi: 10.1007/s10924-016-0795-2.

[100] R. Augustine *et al.*, “Cerium Oxide Nanoparticle Incorporated Electrospun Poly(3-hydroxybutyrate-co-3-hydroxyvalerate) Membranes for Diabetic Wound Healing Applications,” *ACS Biomater. Sci. Eng.*, vol. 6, no. 1, pp. 58–70, Jan. 2020, doi: 10.1021/acsbiomaterials.8b01352.

[101] B. Bal, I. B. Tugluca, N. Koc, and I. A. Isoglu, “On the detailed mechanical response investigation of PHBV/PCL and PHBV/PLGA electrospun mats,” *Mater. Res. Express*, vol. 6, no. 6, p. 065411, Mar. 2019, doi: 10.1088/2053-1591/ab0eaa.

[102] S. Zhong, Y. Zhang, and C. T. Lim, “Fabrication of large pores in electrospun nanofibrous scaffolds for cellular infiltration: A review,” *Tissue Eng. - Part B Rev.*, vol. 18, no. 2, pp. 77–87, Apr. 2012, doi: 10.1089/ten.teb.2011.0390.

[103] G. Mutlu, S. Calamak, K. Ulubayram, and E. Guven, “Curcumin-loaded electrospun PHBV nanofibers as potential wound-dressing material,” *J. Drug Deliv. Sci. Technol.*, vol. 43, pp. 185–193, 2018, doi: 10.1016/j.jddst.2017.09.017.

[104] J. G. Merrell, S. W. McLaughlin, L. Tie, C. T. Laurencin, A. F. Chen, and L. S. Nair, “Curcumin-loaded poly(ε-caprolactone) nanofibres: Diabetic wound dressing with anti-oxidant and anti-inflammatory properties,” *Clin. Exp. Pharmacol. Physiol.*, vol. 36, no. 12, pp. 1149–1156, Dec. 2009, doi: 10.1111/j.1440-1681.2009.05216.x.